Low-Energy Electron Transmission through Thin-Film Molecular and Biomolecular Solids

R. Naaman[†] and L. Sanche*[,‡]

Department of Chemical Physics, Weizmann Institute, Rehovot, Israel 76100, and Groupe en Sciences des Radiations, Département de médecine nucléaire et de radiobiologie, Faculté de médecine, Université de Sherbrooke, Québec J1H 5N4, Canada

Received June 16, 2006

Contents

1. Introduction

1.1. General

Electron transfer is a fundamental chemical process underlying all redox reactions and has been under experimental and theoretical study for many years. Generally, electrons may be transported through organic molecules following various mechanisms. One way to sort the transport processes is by relating them to the energy of the transported electron. For example, in the well-established field of electron transfer, the electron has negative energy relative to the vacuum level (VL) when it is transmitted between the donor and the acceptor through a molecular bridge.[1] In recent years, we have seen the emergence of a new field of study, involving molecular "wires" connecting metal or semiconductor contacts.[2] Here the traditional molecular view of electron transfer between donor and acceptor species gives rise to a novel view of the molecule as a current-carrying conductor, and observables such as electron-transfer rates and yields are replaced by the conductivities of such molecular junctions or, more generally, by a current−voltage relationship.

Another type of transport occurs when the electrons have positive kinetic energy relative to the VL; namely, the electrons are unbound while passing through organic films. Such electrons are applied in electron microscopy, where electrons with energies of thousands of electronvolts are used for obtaining structural information.[3] In the low-energy region above the VL, low-energy electron transmission (LEET) and low-energy photoelectron transmission (LEPET) spectroscopies have provided information on the transport parameters of electrons with energies close to zero to about 12 eV in thin-film molecular and biomolecular solids along with data on their dielectric properties. These techniques and the results obtained from their use with such films since the earliest experiments are reviewed in the present article.

From biophysics to insulation of power lines and futuristic applications of molecular electronics, understanding the transmission of low energy (0−12 eV) electrons (LEEs) through organic-based materials is of central interest. The energy dependence of LEE transmission through dielectric media and semiconducting materials has been investigated both theoretically and experimentally for more than half a century. In such experiments, LEEs are incident on a thin film usually deposited on a metal substrate; simultaneously the current passing through the film is measured as a function of electron energy. Basically, two types of transmission experiments can be performed: LEET and photoinjection. In the photoinjection experiment,[4,5] electrons photoejected from the metal substrate, which pass through the film, are measured in a vacuum. The photoelectrons are injected into the film with ill-defined energies and momenta, but the outgoing electrons that escape into the vacuum with a given energy and momentum can be selected with an electron analyzer. In LEET, electrons from vacuum are incident on the film. In this case, the incident beam has a well-defined energy and momentum, but the current measured at the metal substrate contains electrons scattered into all angles that have lost energy. Furthermore, when the film is highly disordered, electrons are scattered in all possible directions near the surface[6] so that in LEET the momentum of the electrons in the bulk is also unspecified. Both techniques are somewhat complementary: one specifies energy and momentum for incoming electrons and the other for transmitted electrons.

* To whom correspondence should be addressed. Phone: (819) 346-1110, ext. 14678. Fax: (819) 564-5442. E-mail: Leon.Sanche@USherbrooke.ca.
[†] Weizmann Institute.
[‡] Université de Sherbrooke.

10.1021/cr040200j CCC: $65.00
Published on Web 04/18/2007

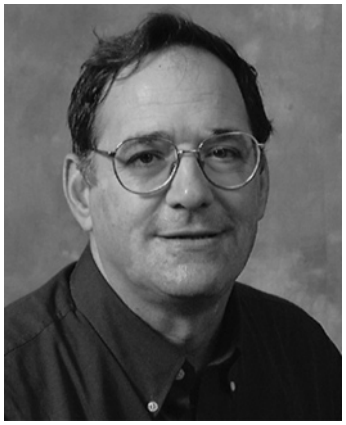

Ron Naaman completed his B.Sc. in Chemistry at the Ben Gurion University, Beer-Sheva, Israel, and his Ph.D. at the Weizmann Institute in Israel. He then moved for postdoctoral fellowship to Stanford, California, for 2 years and then spent 1 year at the Chemistry Department at Harvard. In 1980, he returned to Israel and became a faculty member at the Weizmann Institute. His work is focused on new electronic properties that emerge from the formation of supramolecular structures. He studies the effect of formation of clusters and van der Waals complexes on the reactivity of molecules. This work was followed by studies of reactive properties and electronic properties of self-assembled monolayers. In parallel, his research group explores the transfer of information through supramolecular systems and produces self-assembled electrical devices.

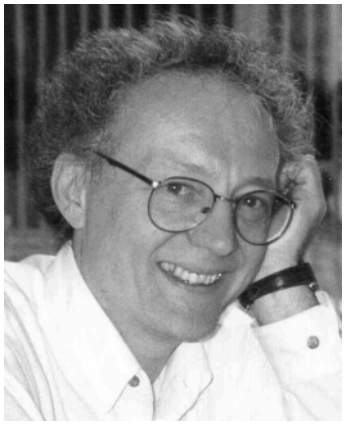

Professor Sanche graduated from Yale in 1972. His general career goal has been and still is to achieve a global comprehension of the effects of radiation in biological systems and to apply this knowledge to enhance the therapeutic and diagnostic efficiency of radiation. To work efficiently toward this general objective, he formed in 1982 a group of the Medical Research Council of Canada. His investigations have been essentially focused on the action of secondary electrons generated by high-energy radiation in condensed matter, particularly in biological tissue. More specifically, he worked on the physics and chemistry of low-energy electrons in organic and biomolecular solids, DNA damage, and radiosensitizers, as well as in the applications of LEE interactions to other fields such as ballistic electron transport in nanoscale circuits and field-effect devices, nanolithography, planetary and atmospheric science, photoelectron-induced surface chemistry, and dielectric aging in high-voltage cables. In 1997, he obtained a Distinguished Scientist Award from the Medical Research Council of Canada and in 2002, a senior Canadian Research Chair in the Radiation Sciences in recognition of most of these advances.

Theoretically, in the simplest approach, it was assumed that the electron is a point charge and scatters in the medium via classical mechanics.[7] With this formulation, the energy dependence of the elastic and inelastic mean free paths (MFPs) can be estimated. This classical approach is based on random scattering processes, in which electrons change their momentum because of the collision with atoms or molecules. Under such conditions any initial energy distribution becomes broader and some of the transmitted electrons have a lower energy than their initial energy (see Figure 1). It is also possible, in a different approach, to parametrize the dielectric by a barrier and to calculate the tunneling probability through this barrier. In this quantum mechanical approach, the problem is treated in one dimension and the barrier is characterized by its height and width.[8] Full quantum mechanical simulations have been conducted on electron transfer through thin argon[9,10] or water layers. In these simulations, the "band"-like electronic structure was established for ordered layers.[11] A comprehensive review of the theoretical aspects of electron transmission through molecular interfaces has recently been published by Nitzan.[12]

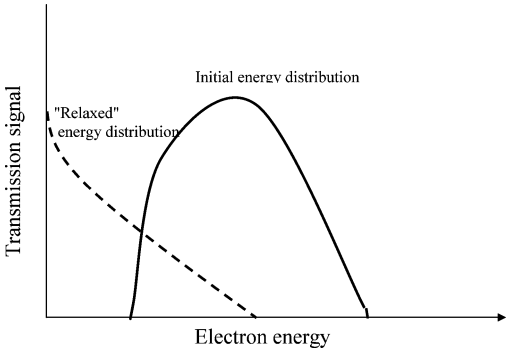

Figure 1. The expected transmitted photoelectron energy distribution assuming "classical" scattering of electrons by molecules in a thin film deposited on a metal substrate (dashed line). The initial photoelectron spectrum from the metal substrate is shown as a solid line.

1.2. Low-Energy Electron Transmission (LEET) Spectroscopy

Despite their simplicity, LEET experiments have often been difficult to interpret owing to multiple scattering of the electrons. In the past, several attempts have been made to correlate structure appearing in current vs voltage plots of the transmitted current with the target band structure (i.e., the relationship between electron energy, momentum, density of electron states, and geometrical structure). In the early work of Hilsch,[13] Wright,[14] and Bruning,[15] low-velocity electrons were used to bombard metal surfaces coated with thin films of potassium chloride, sodium chloride, calcium fluoride, and barium oxide targets. The ratio of total backscattered current (elastic plus inelastic) to the bombarding current was measured as a function of electron energy. Since the transmitted current represents the incident current minus the total reflected current, these experiments are equivalent to LEET experiments. In all backscattering measurements, a decrease in emitted electrons (corresponding to an increase in transmission) was noted at a certain critical energy for each particular film. From comparisons with optical absorption experiments, it has been found that exciton levels existed near maxima in the transmitted current. More systematic investigations were later performed by Jacobs et al.,[16] Fredrikov and Goryacheva,[17] and Fredericks and Cook,[18] who interpreted structure in their spectra as electron interaction with crystal imperfections. In the 1970s, LEET experiments in pure[19,20] and doped[21] alkali halide films, as well as alkaline earth fluoride films,[22] were performed by Hamill and coworkers. Above the lowest energy optical transition, maxima in the first energy derivative of the transmitted current were interpreted to result from electronic transitions. Structures below the lowest energy optical transition were attributed to the formation of triplet excitons and to electron interaction

with imperfections or degraded molecules. Molecular solids in the form of organic films were also investigated by Hiraoka and Hamill.[23,24] At lower energies, LEET features were attributed to the presence of temporary negative ions or pre-existing trapping potentials. Later, Hiraoka and Nara[25] suggested that the 0−2 eV features in hexane, ethers, and alcohols could arise from electron tunneling to the metal substrate through a negative potential barrier.

Starting in 1979, organic molecular films were reinvestigated,[26,27] using an electron monochromator as a source instead of a simple filament. In these experiments, electrons were collimated by a magnetic field to align the electrons. Because of these advances in the technique, the visibility of sharp structures was enhanced, and their energies were more accurately defined. For example, it was possible to observe a larger number of structures for a given target and to make accurate comparisons with energy levels found by other spectroscopic methods. Such comparisons, combined with theoretical calculations, made it possible to unambiguously identify the origin of the structures found in LEET spectra and to develop procedures to analyze the data. Today, the underlying mechanisms in LEET spectroscopy are fairly well understood. One can delineate two regimes in LEET spectra: the collective regime below the energy threshold for electronic excitation of the molecules within the film, and the inelastic regime above this energy. A structure appearing in the former is usually due to elastic and quasi-elastic scattering (i.e., electron energy losses to phonons), whereas in the latter regime electrons having electronically excited the target atoms or molecules produced the observed LEET features. The elastic and quasi-elastic features are generally related to the electronic conduction-band structure above the vacuum level[28−34] and hence are sensitive to structural order[35−38] and film thickness.[28−30,32,37] For very thin ordered films, quantum interferences of the electron wave between the vacuum−film and film−substrate boundaries, called quantum size effects (QSEs),[28,30,39,40] appear in the elastic portion of the transmitted current. The inelastic features in LEET spectroscopy usually appear as broad maxima[6,35,41] resulting from a convolution of inelastically scattered current distributions created by electrons having lost most of their energy from producing electronic excitations and band-to-band transitions. With this knowledge, LEET spectroscopy has been applied to diverse problems.

By monitoring the thickness and energy dependences of the "elastic" features (i.e., those in the collective regime that arise from elastic and quasi-inelastic scattering), it was possible to characterize film growth including the determination of their thicknesses,[28,30,39] orientations,[28,32] layer-by-layer constructions,[28,30,32,42] and phase changes.[36] The formation of defects[6,31,41,43−45] and quantum well structures[29] in thin films has also been detected by LEET spectroscopy. Studies involving the inelastic features served to identify spin-forbidden electronic transitions having strong threshold cross sections within molecular solids.[6,31,41,44,45] These measurements also led to estimates of inelastic cross sections near the threshold[45] and of the energy of the lowest conduction level, V_0 (i.e., the energy of the band edge near the vacuum level below which electrons have no energy states in the solid) in several molecular[6,35,43] and organic solids.[46,47] Furthermore, in experiments where the primary particles are LEEs incident from vacuum on a solid surface, LEET spectroscopy can be used on a routine basis to monitor film charging,[48] metal work function changes,[38,49,50] and chemical degradation.[51] It is also possible to calibrate the electron-energy scale with respect to the VL[52,53] by measuring the energy onset of the transmitted current.

1.3. Low-Energy Photoelectron Transmission (LEPET) Spectroscopy

The early low-energy (0−10 eV) photoinjection experiments have been performed essentially to obtain information on the scattering length, escape depth, or MFPs of LEEs in molecular films.[54−75] These parameters could be determined by measuring the intensity of the current transmitted into vacuum as a function of film thickness. Depending on the experiment, either the transmitted current[55,62] or its entire energy distribution[63,64,74,75] was measured. The analysis of the full thickness dependence of the transmitted substrate current intensity with appropriate mathematical models[56,70] often yielded determination of both inelastic and elastic scattering lengths or MFPs from the measured attenuation lengths. This sort of photoinjection experiment is now well established as a method to measure parameters related to LEE scattering MFPs in insulators and semiconductors. For further information on the results obtained with this technique, the reader is referred to the review article by Marsolais.[4]

As the field progressed, investigators became preoccupied with the band structure properties of the phototransmitted current, which led to the development of LEPET spectroscopy. In this spectroscopy, the photoelectrons are also ejected by light from a conductive substrate coated with a thin organic molecular film, but the main focus of the experiment is to investigate the details of the energy and angular distribution of the photoelectrons transmitted into vacuum and their relationship to the band structure. Although, as opposed to LEET, there is a very limited control of the initial parameters of the electrons in LEPET, before they are ejected into the organic layer; parameters related to intensity, momentum, and energy can be measured in detail for post-transmission electrons. As will be shown in subsequent sections, such a detailed analysis of LEE transport properties by LEPET spectroscopy has revealed a large number of structural and electronic properties of organic thin films from simple molecular solid films to systems as complex as DNA.

Recently, the electronic properties of adsorbed organic molecules have been investigated by two-photon LEPET spectroscopy. Experiments have been performed both with subpicosecond[76,77] and with nanosecond laser pulses.[78] In these studies, the first photon excites electrons in the substrate, which can transfer them to either a surface state or a negative ion state on the adsorbate. A second photon detaches the electron from the metastable state and, when this electron is transmitted to vacuum, its kinetic energy and angular distribution are measured. Two-photon LEPET has been used to study the electronic structure of the adsorbed layer,[79] the nature of the electronic states,[80] and the interaction between the adsorbates and the metal substrate.[81]

2. Experimental Methods

2.1. LEET Spectroscopy

In the LEET technique, spectra are recorded with an apparatus of the type shown in Figure 2, which is housed in an ultrahigh vacuum (UHV) system. Basically, it consists of a trochoidal monochromator, a pair of deflector plates, D, and a cryostat, L. Electrons exiting the monochromator are deflec-

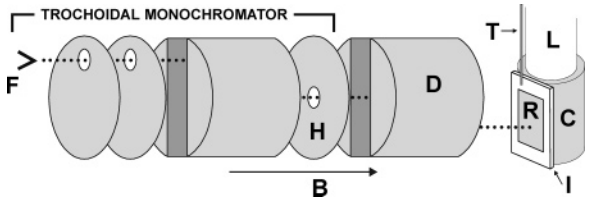

Figure 2. Schematic diagram of a low-energy electron transmission (LEET) spectrometer. Electrons emitted from the filament F are aligned by a magnetic field **B**, and energy is selected by a trochoidal monochromator. The monoenergetic electron beam is then deflected off-axis by passing it through an electric field applied across the parallel surfaces D. The deflected beam is incident on a thin molecular film deposited from the vapor on a metal ribbon R. This metal ribbon is electrically insulated from a copper block C by a ceramic sheet I. The copper block is maintained at cryogenic temperature. The portion of the incident current transmitted through the molecular film, or the negative value of its second energy derivative, is measured as a function of electron energy. Reprinted from ref 27, Copyright 1979, with permission from Elsevier.

ted by plates D and impinge on a molecular film condensed on a metal ribbon, R. The current transmitted to the metal substrate is measured as a function of electron energy, *E*. The cryostat consists of a liquid-nitrogen-cooled stainless steel finger or a closed-cycle helium-refrigerated system ending with a copper block. A metal ribbon is secured by a press fit to a pure ceramic sheet that is attached to the copper block. Metal shielding is placed around the ribbon to prevent electrons from reaching the ceramic. Electrical leads spot-welded across the metal ribbon provide connections for cleaning the substrate by resistive heating and are used for measuring the electron current. Molecules admitted in vapor form through tube T are condensed on the ribbon R. Films of materials that exhibit a high vapor pressure are grown using a gas-volume expansion dosing procedure[26] that can be calibrated by monitoring the QSE features observed for ultrathin films.[28] Films of materials that under ambient conditions might be described as low-vapor-pressure solids can be grown using an oven to generate a low-density molecular flux.[82]

In the trochoidal monochromator,[83] electrons emitted from a filament F are aligned by an axial magnetic field **B** of 50 G. Two electrodes following the filament have holes drilled off-center. Thus, electrons enter the set of parallel plates off-center. In this region, an electric field **E** perpendicular to **B** is established by applying a small potential across the two parallel surfaces. In the crossed-field region, the electrons describe a trochoidal motion and their guiding center moves with a velocity $\mathbf{E} \times \mathbf{B}/B^2$. They are dispersed according to their axial velocities and those that reach the center of the tube are transmitted through the exit hole (H). The monoenergetic electrons are accelerated by a potential of about 30 V into another pair of parallel surfaces D, where they are further deflected by application of a potential difference across the surfaces. Thus, electrons hit the target off-axis. An interesting characteristic of the motion in such a cross-field region is that the $\mathbf{E} \times \mathbf{B}$ drift experienced by the electrons takes place in the same direction,[83] regardless of the direction of motion along the axis of the tube. That is, electrons that scatter from the target and enter the parallel surfaces acquire a drift in the same direction as those entering at electrode H.[84] Since the magnetically confined electrons always travel along the direction of the axis of the tube, unless acted upon by the $\mathbf{E} \times \mathbf{B}$ force, this arrangement prevents any electrons that have scattered once from the target R from reaching it again. Scattered electrons end up traveling on an axis out of the target range. Eventually, they are collected by metal surrounding the spectrometer. *With this type of device, all scattered electrons are dispersed outside the target region*. These precautions are important to produce LEET spectra free from artifacts created by reflected electrons. *Furthermore, since the current intensity of magnetically confined electron beams is independent of energy at low current densities, the magnitude of the transmitted current becomes a quantitative determination of the overall transmission coefficient*. Since the transmitted current is equal to the incident current minus the total reflected current, under these conditions, LEET spectra exhibit the inverted line shape of the total reflected current.

Electrons are accelerated to the film by a ramp voltage placed between the metal substrate and the monochromator. They arrive at the film surface with kinetic and total energy *E* defined with respect to VL. The latter is determined by measuring the position of the steepest slope in the current onset of the transmitted current (i.e., the injection curve). As explained in section 6, a shift toward higher energies of this current onset is due to charging of the film by trapped anions or electrons. Before and after the recording of a LEET spectrum, the injection curve is measured in order to verify whether charging occurs. When the shift is larger than the energy resolution of the monochromator, the curve is discarded, even though such a shift does not affect the line shape of LEET spectra at energies above those of the injection curve. In a typical LEET experiment, the time required to record a spectrum varies from about 0.1 to 10 min; the monochromator provides an electron current of between 1 and 10 nA, with an intrinsic resolution between 40 and 60 meV full width at half-maximum. Under these conditions, film decomposition is negligible as verified by the absence of change in the line shape of repeated LEET spectra on the same film.[26,35] The beam is incident normally on the film surface. The absolute energy scale is calibrated to within ± 0.15 eV of the VL and the film thickness to 30−50% accuracy.

2.2. LEPET Spectroscopy

In a typical LEPET experiment, an organic film is deposited on top of a conductive substrate and placed inside an ultrahigh vacuum chamber.[85,86] Various lasers can be used to eject photoelectrons from the conducting substrate. The energy and angular distribution of electrons that pass through the organic film are measured in vacuum.

The lasers' wavelengths are chosen such that the photon energy is above the substrate work-function but below the ionization potential of the molecules so that all the electrons originate from the conductive substrate. Typically, the photon energy is chosen not to be absorbed by the film. The power in the laser pulses is kept sufficiently small to avoid charging of the film by electrons and to avoid any nonlinear effects.

The laser beam is introduced into the vacuum chamber, and after being reflected from the sample, it exits through quartz windows. The photoelectron kinetic energy distribution can be measured by various electron energy analyzers. In order to avoid light-induced or charge-induced damage to the film, it is preferable to use a time-of-flight electron energy analyzer that provides the full electron energy spectrum for every laser pulse. This technique enables shorter collection time thereby avoiding decomposition of the molecules forming the organic films.

3. Interpretation of LEPET Experiments

When electrons are ejected from a conductive substrate their energy distribution, $P_0(E)$, depends on the photon

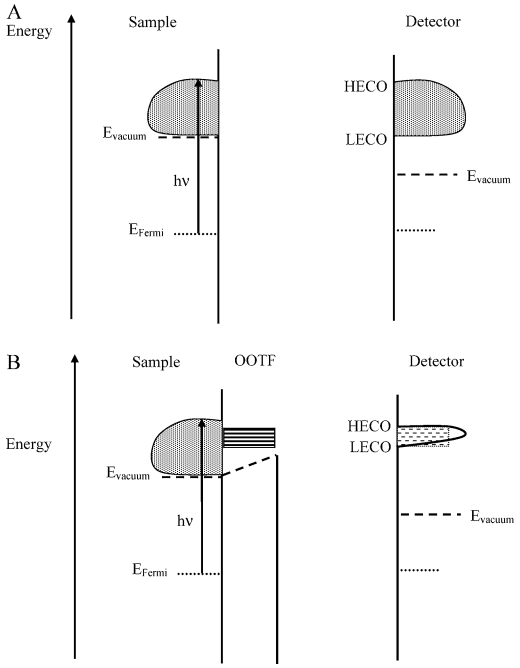

Figure 3. Energy level diagram for photoelectron transmission. The Fermi level of the system is shown as a dotted line, whereas the vacuum level of the sample (on the left) and the detector (on the right) are shown as dashed lines. The photoelectron energy distribution is shown for a bare substrate (A) and for a substrate coated with OOTF (B). The low-energy cutoff of the distribution is denoted as LECO. The transmission probability through the film (B) modifies the spectrum of electrons. The high-energy cutoff (HECO) is defined by the photon energy ($h\nu$) and the work function of the detector and is insensitive to the substrate work function (A). The resonance states of the OOTF are shown in panel B as solid black−white lines.

energy, the density of states in the substrate, the barrier for electrons to escape from the substrate (work function), and the work function of the detector. Special attention is given to the low- and high-energy cut-offs (LECO and HECO, respectively) in the energy distribution of transmitted electrons (see Figure 3A). The LECO depends on the work function of the substrate and the difference between it and that of the detector. The HECO is a function only of the photon energy and the electron affinity of the detector (see Figure 3A). When an organic layer is adsorbed on the surface, its work function may be changed by exchanging charge with the substrate or by applying force on the ejected electrons, due to the intrinsic dipole moment of the molecules on the layer. Afterward, the LECO depends on the new work function of the metal−film system (see Figure 3B). In addition, there is an energy-dependent probability, $T(E)$, for electrons to be transmitted through the layer. Hence the final energy distribution of the electrons, $P(E)$, is given by

$$P(E) = P_0'(E)T(E) \tag{1}$$

when $P_0'(E)$ is the *modified energy distribution* of the photoelectron ejected from the substrate due to the chemical bonding of film. From eq 1, it is clear that in LEPET studies $T(E)$ cannot be obtained simply by measuring $P(E)$ and that of the pure substrate, $P_0(E)$, since $P_0' \neq P_0$. Still, as will be shown, LEPET provides direct information about the electronic properties of the adsorbed film.

The energy distribution $P(E)$ evolves according to film thickness depending on the different parameters, which

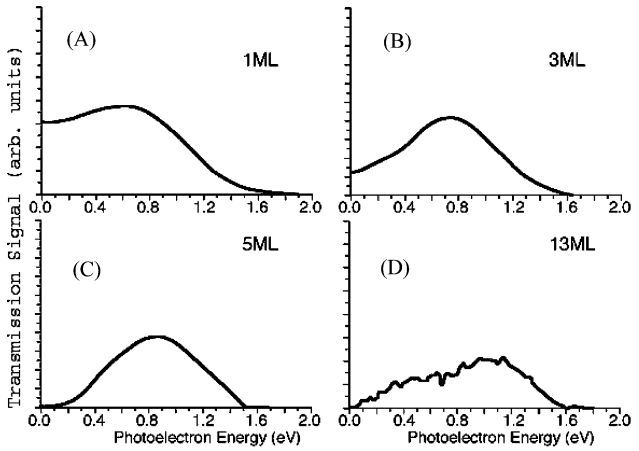

Figure 4. The electron energy distribution of photoelectrons from gold coated with one (A), three (B), five (C), and thirteen (D) monolayers of cadmium stearate. Reproduced with permission from ref 87. Copyright 1997 John Wiley & Sons Limited.

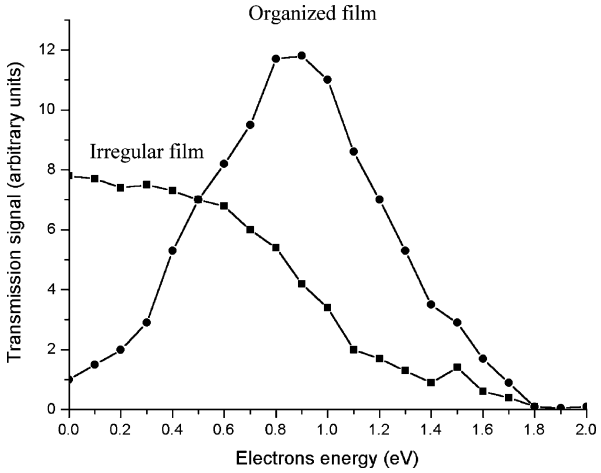

Figure 5. The current density as a function of electron energy for photoelectrons transmitted through 13 layers of Cdar before (●) and after (■) they were heated to 378 K and cooled back again to room temperature. Reproduced with permission from ref 87. Copyright 1997 John Wiley & Sons Limited.

influence $T(E)$. For instance, as explained elsewhere in this article, as the film gets thicker electrons are increasingly scattered in all directions leading to LEPET spectra that are increasingly related to the film band structure. Such an evolution of $P(E)$ is shown in Figure 4 for photoelectrons emitted from a gold substrate coated with one (A), three (B) and five (C) monolayers of cadmium stearate (Cdst). Also, as the film thickness increases the number of electrons transmitted having energies close to thermal energy increases; eventually, at high thicknesses, we have a "relaxed" energy distribution similar to that shown in Figure 1. In fact, it can be seen from Figure 4D that such a relaxation is beginning to occur at 13 ML thickness causing a relative increase of transmitted current around 0.4 eV and depletion of this current at higher energies. Another parameter that influences LEPET spectra is film order. An example is shown in Figure 5, which presents the current as a function of electron energy for photoelectrons transmitted through 13 layers of Cdar [cadmium salts of arachidic acid], before (circles) and after (squares) they were heated to 378 K and cooled back again to room temperature. Thus, before heating, electrons with energies near ca. 1 eV are transmitted through the band very efficiently with little energy loss. Following heating, the electron energy distribution indicates that extensive random

scattering processes have occurred as one can observe a strong increase in the population of electrons at low energies. This is an indication that a relaxed distribution evolved due to inelastic scattering of electrons in the film.

The results presented above indicate a "nonclassical" scattering process that can in principle result from two different effects. One is related simply to the fact that thin layers exist with thicknesses comparable to the electrons' wavelength; hence electron interferences in the transmission result in specific structures.[28] These interferences are very sensitive to the thickness of the layer but only weakly depend on the electronic properties of the molecules. Another source for the structure in the transmission spectrum may arise from formation of a transient negative ion state,[84] which is due to the temporary localization of an incident electron in a usually unfilled orbital of a molecule in the film. Since the radius of the electron's orbital in these states is large, it causes coupling with nearby molecules in the layer and electronic bands are formed. In both cases, the layer must be well-organized.

The positions of the maxima of the distributions in Figure 4 are almost independent of the thickness of the films (one, three, or five layers).[87] This is *inconsistent* with quantum interferences and indicates that the band structure is controlling the electron transmission. The transmission indeed depends on the films being well organized. Since these latter are Langmuir−Blodgett films, they melt upon warming, and ordering of their constituents is lost. The same conclusion has been reached based on LEET studies, which are described in the next section.

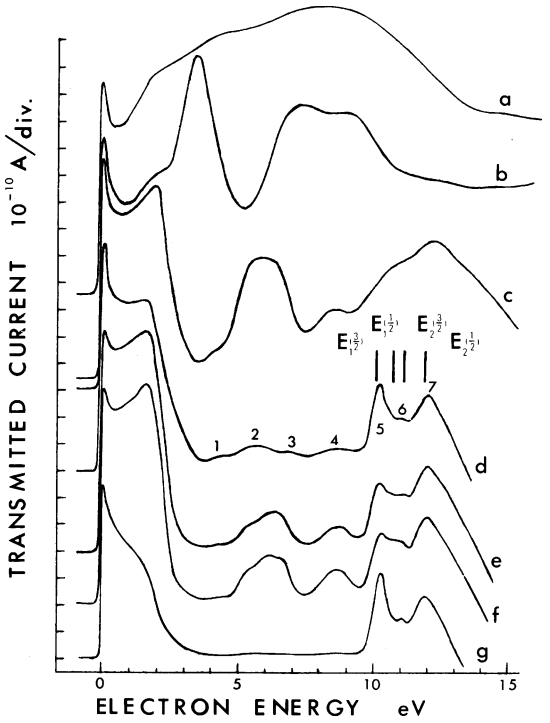

Figure 6. LEET spectra of single layer (b) and multilayer Kr films (c−g). Curve a represents the current at the bare platinum substrate. The vertical lines represent the energies of the lowest excitons. Reused with permission from L. Sanche, G. Perluzzo, G. Bader, and L. G. Caron, *Journal of Chemical Physics*, *77*, 3285 (1982). Copyright 1982, American Institute of Physics.

4. Measurements of Elastic and Quasi-Elastic Scattering in Thin Films by LEET

"Elastic" scattering within thin dielectric films has been investigated by analyzing the elastic and quasi-elastic contribution to the LEET current[28,33,36,39,43,45,88−99] within the collective regime. However, even when elastic scattering dominates, such an analysis is not straightforward, since the LEET current is not simply the complement of the currents arising from the addition of the specular and diffracted beam intensities, which constitute the purely elastic portion of the transmitted intensity. Other currents that form the quasi-elastic contribution arise from scattering at the boundary of the microcrystals and scattering by defects, imperfections, and phonons. Figure 6 shows, as an example, LEET spectra for Kr films deposited on a polycrystalline platinum substrate.[100] Recording such spectra at different film thicknesses and temperatures allows one to differentiate between elastic, quasi-elastic, and inelastic scattering. Curve a was recorded for the clean metal, whereas curves b, c, d, and g represent the energy dependence of the current transmitted through Kr films of 1, 10, 100, and 500 monolayers (ML), respectively, deposited and held at 17 K. Curves e and f were recorded at a 100 ML coverage. For curve e, the temperature was kept constant at 31 K during the deposition and the experiment. Curve f was recorded at 17 K after deposition at 31 K. As the Kr film becomes thicker, features 1−4 progressively disappear and features 5−7 become sharper. Feature 3 also shifts to higher energy with increasing thickness. The maxima in features 5−7 correspond within ±0.2 eV to the position of the first two excitonic levels ($n = 1$ and 2) of the $J = {}^1/_2$ and $J = {}^3/_2$ series of solid krypton,[101] which are represented by vertical bars in the figure. In the two-stream approximation,[45] the inelastically scattered current is predicted to be independent of thickness at large thicknesses, whereas, under the same conditions, the elastic and quasi-elastic currents become inversely proportional to the thickness. This behavior is observed for structures 5−7 and 1−4, respectively. An elastic/quasi-elastic behavior below 10 eV is expected, since only acoustic phonons can produce energy losses in this range.[102] Structures 1−4 were also found to depend on the ordering of the Kr film. The films deposited at 17 K (curve d) are the most disordered ones (structural disorder). In the film deposited at 3l K (curve e), the structural disorder is smaller, but there is greater thermal disorder (phonons) than in the 17 K-deposited films. The films deposited at 3l K and cooled to 17 K (curve f) are the most ordered ones: a low structural disorder because of the high deposition temperature and a low thermal disorder, since at 17 K the phonon population is greatly reduced (Debye temperature 64 K).[45] The structures below 10 eV are therefore closely related to the ordering of the films. Finally, when a single layer of Kr is deposited (curve b), quasi-elastic scattering becomes negligible and interferences of the incident electron wave between the interfaces dominate the spectrum. For this reason, curve b in Figure 6 is different from all others due to the prominence of purely elastic scattering.

More detailed analysis of the LEET spectra of Ar, Xe, and CH_4 films, according to the Fermi golden rule, has been performed by comparing the experimental results with the respective electronic conduction band density of states (CBDOS) calculations,[33,89,92,93] which provides the density to energy levels (averaged over all directions) available to electrons as a function of energy. These comparisons clearly indicate a relationship between the quasi-elastic LEET current in the collective regime and the CBDOS of the solid, as shown for the case of Ar films[93] in Figure 7. Here, the

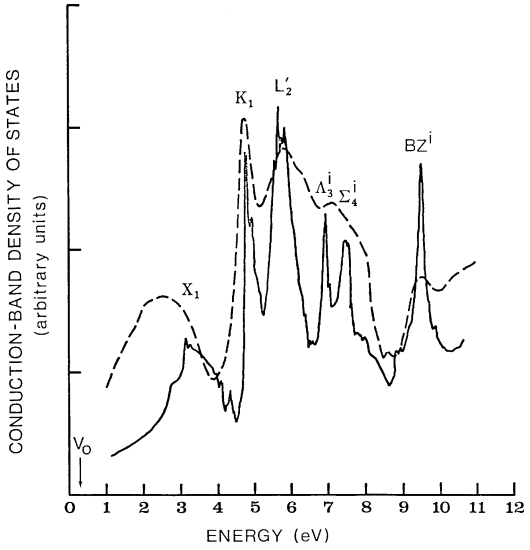

Figure 7. Electron conduction-band density of states (CBDOS) of solid argon, calculated (full line) and determined from analysis of LEET data for solid argon recorded at ~ 20 K. The zero of energy is that of the vacuum level (VL); V_0 is the energy of the bottom of the conduction band. The letters on top of each peak represent the designation of the corresponding band features. Reprinted from ref 93, Copyright 1988, with permission from Elsevier.

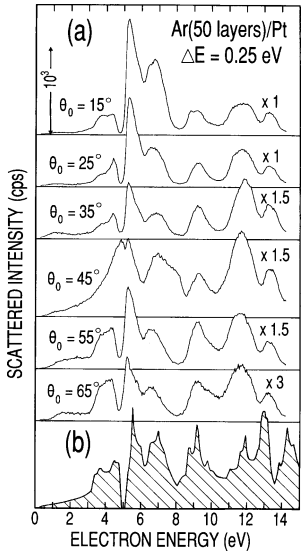

Figure 8. (a) Analysis of electrons, which are backscattered from a 50 ML Ar film, after having lost $\Delta E = 0.25$ eV. Scattered electron intensity is shown as a function of the incident electron energy for several angles of incidence, θ_0. Reprinted with permission from ref 106 (http://link.aps.org/abstract/PRB/v44/p10485). Copyright 1991 by the American Physical Society. (b) CBDOS for the fcc structure of solid Ar, as calculated by Bacalis et al. Reprinted with permission from ref 108 (http://link.aps.org/abstract/PRB/v38/p6218). Copyright 1988 by the American Physical Society.

CBDOS calculated by the linear analytic tetrahedron method[103] is represented by the solid line. The CBDOS extracted from the LEET spectrum is represented by the dashed line.[93] It was derived from the theoretical model developed by Plenkiewicz et al.[88] to explain the transmission of low-energy electrons though condensed multilayer films. In this model, the transmission of incident electrons through a thin dielectric film of thickness d is considered to be a two-step process. To begin with, electrons after being scattered in passing through the vacuum−film interface penetrate the surface potential barrier of the film in proportion to the film's three-dimensional electronic CBDOS, $D(E)$. Subsequently, they propagate (in Bloch states) into the film in all possible directions in a manner that is characterized by a MFP $\lambda(E)$. Under the condition $\lambda(E) \gtrsim d$, the total transmitted current, $I_t(E)$, is given by

$$I_t \propto I_0 \frac{D}{\sqrt{E}}(1-R)\left\{\beta\left[1-\left(\frac{1-\beta}{\beta}\right)\left(\frac{d}{\lambda}\right)E_1\left(\frac{d}{\lambda}\right)\right]+(1-\beta)\,e^{-(d/\lambda)}\right\} \quad (2)$$

where I_0 is the intensity of the incident electron current at the target, $R(E)$ is a slowly varying function of E that describes the reflection coefficient of the injected electron at the film−metal boundary, β is an energy-dependent adjustable parameter representing the number of scattered electrons that reach the metallic collector, and

$$E_1\left(\frac{d}{\lambda}\right) = \int_1^{\infty} \frac{\exp[-(d/\lambda)t]}{t}\,dt$$

By fitting the experimental thickness dependence of $I_t(E)$ to eq 2, one can calculate both the electron MFP and the electronic CBDOS as a function of energy. A further correlation between the electronic CBDOS and the "elastic" (i.e., elastic and quasi-elastic) features in the collective regime has been achieved[36] by comparing the "elastic" features with the structure in secondary electron spectra, which were previously shown[104,105] to reflect changes in the CBDOS. In other experiments, the smearing out of LEET features near the melting point of long-chain alkane films[36] was attributed to smoothing of the CBDOS due to the breakdown of the intermolecular symmetry (e.g., phase transitions) induced by thermal excitations. Changes of the electron effective mass with energy have also been invoked by Plenkiewicz et al.[33,88] to explain the energy dependence of the MFP in the collective regime.

When films are sufficiently disordered, the correspondence between LEET features in the collective regime and the CBDOS can generally be traced to multiple phonon losses, which scatter electrons in all directions within the film and at its surface. This relationship has been clearly shown by high-resolution electron energy loss spectroscopy (HREEL) on thin rare gas and N_2 films.[106,107] Taking again the example of an Ar multilayer film, this relationship is shown in Figure 8. The curves in the figure were recorded with a HREEL spectrometer set to measure the dependence of energy loss on incident electron energy ($\Delta E = 0.25$ eV) electrons backscattered from the films. The data were recorded at several incidence angles (θ_0) between 15° and 65°. Therefore, these curves represent the probability of an electron, penetrating a 50-layer film of Ar deposited on Pt, to lose 0.25 eV via multiple losses to phonons in the solid. Except for the measurement at $\theta_0 = 45°$ (i.e., in the specular direction), all the features are found generally at the same energy, independent of the incident angle. The similarity between these curves reveals an electron-scattering property of the solid that is averaged over various directions of electron propagation (i.e., various electron states), which may consequently reflect the CBDOS. In Figure 8b, the CBDOS of Ar, as calculated by Bacalis et al.,[108] is displayed with the bottom of the lowest conduction band fixed at the measured value[36,52] of 0.25 eV above the VL. As one can see, the experimental curves of Figure 8a, and especially those for

large incident angles, closely resemble the CBDOS. The closer agreement at large θ_0 presumably arises from a better averaging over the incident direction owing to the disordered arrangement of the deposited polycrystalline films. With the exception of the peaks around 9 and 12 eV, all the calculated features appear progressively shifted to higher energies with respect to the experiment, by ~0.25 eV at low energies to ~1 eV at the highest energy. In this regard, note that the calculations have been performed with a face-centered cubic lattice parameter of 0.526 nm, whereas a larger value of 0.531 nm (typical of solid Ar between 4 and 20 K)[109] would have yielded a more compact density of states[110,111] and consequently an overall better agreement.

One can explain the similarity between the experimental results and the calculated CBDOS by focusing on the electron transport properties in the bulk.[112] An electron propagating in a conduction band of a rare gas solid suffers scattering mainly from defects and lattice waves (i.e., the electron−phonon interaction). This can be described by introducing the scattering probability per unit length, $Q(E_{\mathbf{k}_0},\mathbf{k}_0,E_{\mathbf{k}},\mathbf{k})$ that a Bloch electron initially in a state $|\chi\rangle$ of momentum $\mathbf{k}_0$ and energy $E_{\mathbf{k}_0}$ is scattered into a final state $|\chi_{\mathbf{k}}\rangle$ of momentum $\mathbf{k}$ and energy $E_{\mathbf{k}}$, while the crystal changes from a state $|\mathrm{i}\rangle$ of energy ϵ_i to a state $|\mathrm{f}\rangle$ of energy ϵ_f. Then, by referring to the "golden rule" and solving the Boltzmann transport equation for a plane-parallel system in the "two-stream" approximation,[45,113,114] one obtains for the electron MFP, $\lambda(E_\mathrm{i})$ (i.e., the reciprocal of Q) the expression

$$\lambda(E_\mathrm{i}) \equiv \langle[\sum_{\mathbf{k}} Q(E_{\mathbf{k}_0},\mathbf{k}_0,E_{\mathbf{k}},\mathbf{k})]^{-1}\rangle_{E_\mathrm{i}} \qquad (3)$$

where E_i is the incident electron energy.

In this expression, the $\mathbf{k}$ summation extends over the first Brillouin zone, whereas $\langle ... \rangle$ stands for the average over the incident direction $\mathbf{k}_0$ for a constant incident energy $E_{\mathbf{k}0} = E_\mathrm{i}$. If we replace the summations with integrations and assume for simplicity that the matrix element for calculating Q depends only on the momentum transfer (i.e., $|\mathbf{k} - \mathbf{k}_0|$), eq 3 yields

$$\lambda(E_\mathrm{i})^{-1} = D(E_\mathrm{i})\left[\frac{8\pi^3\hbar}{\Omega S(E_\mathrm{i})}\frac{1}{\tau(E_\mathrm{i})}\right] \qquad (4)$$

where $D(E_\mathrm{i})$ is the CBDOS of the solid at the energy E_i, $\tau(E_\mathrm{i})$ corresponds to a relaxation time (i.e., the time between scattering events) independent of the $\mathbf{k}_0$ direction, $S(E_\mathrm{i})$ is the surface of constant energy E_i within the first Brillouin zone, and Ω is the volume of the crystal. Within the approximations of an electron effective mass and of an electron−phonon interaction described as a deformation-potential perturbation, one has[115] $1/\tau(E_\mathrm{i}) \propto |\mathbf{k}_0|^2$ and $S(E_\mathrm{i}) \propto |\mathbf{k}_0|^2$. Consequently, the expression in parentheses in eq 4 is independent of E_i, and the energy dependence of $\lambda(E_\mathrm{i})^{-1}$ or Q (i.e., the quasi-elastic scattering probability per unit length) becomes directly proportional to the CBDOS, as shown experimentally in Figure 8.

The examples of (a) *n*-hexane and (b) ethyl-benzene in Figure 9 show how the CBDOS features in a LEET spectrum reflect changes in the geometrical arrangement of the molecules in films.[49] The vertical axes in the figure represent the transmitted current I_T, whereas the horizontal axis corresponds to *uncorrected* electron energy. By this we mean that only the energy scales in the bottom curves of Figure 9a,b have been calibrated, as described at the end of section 2.1. The other curves have not been adjusted to VL = 0 eV in order to make changes in the surface work function visible. The nominal film thicknesses were 6 ML for *n*-hexane and 12 ML ethyl-benzene. For each spectrum, a new film was deposited at the indicated temperature. As shown for Kr films, the spectra of Figure 9 depend on the film's geometrical arrangement; we therefore expect the structure in the collective regime to be altered considerably if the structural order is changed. This can occur, for example, when annealing of an amorphous film at an appropriate temperature forms a crystalline solid. Since the CBDOS of amorphous materials is less defined in energy than that that of crystalline solids, we expect the LEET spectra[116,117] of amorphous films to exhibit broad features, as seen in Figure 9b, and those of crystalline films to have a much sharper structure, as seen in Figure 6.

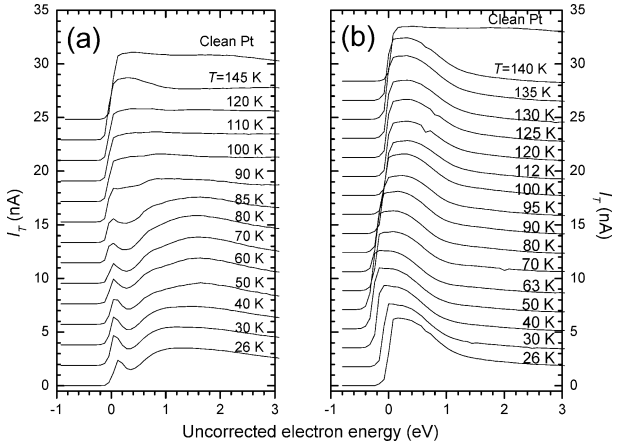

Figure 9. LEET spectra for (a) 6 ML of *n*-hexane deposited at temperatures *T* between 26 and 145 K and (b) 12 ML of ethyl-benzene deposited at *T* between 26 and 150 K. Reused with permission from A. D. Bass, L. Parenteau, F. Weik, and L. Sanche, *Journal of Chemical Physics*, *113*, 8746 (2000). Copyright 2000, American Institute of Physics.

For the case of *n*-hexane in Figure 9a, a significant change in the LEET spectrum is observed between the temperatures of 85 and 100 K. For temperatures of 90 K and lower, a dip is present in the LEET spectra near 0.4 eV, which is due to the negative electron affinity of *n*-hexane films[43] (i.e, the fact that the lowest conduction level of *n*-hexane lies above the VL). Since *n*-hexane has a conduction-band edge (i.e., the energy of the bottom of the conduction band, V_0) lying 0.8 eV above VL, the LEET current decreases as E is reduced from ~2 to ~0.4 eV, since electrons cannot be transmitted easily through the band gap. As explained by Caron et al.,[43] below this latter energy, the LEET current recovers owing to electron conduction via gap states. Thus, the disappearance of this feature above 90 K in the present experiment is indicative of a reduction in the V_0 level of *n*-hexane. It has been estimated that V_0 is less than 0.2 eV for *n*-hexane films above 100 K. Since calorimetric measurements[118,119] for vapor-deposited *n*-hexane indicate that a transition from the amorphous to the crystalline phase is in the same temperature range, this marked change in the LEET spectra can be attributed to this transition.[43,120] Additionally, a 0.2 eV reduction in the surface work function is visible in the LEET current onset as the deposition temperature T increases to 145 K.

In contrast, no significant change was observed in the line shape of LEET spectra obtained for ethyl-benzene films with deposition temperatures between 26 and 140 K. This suggests that no change of phase occurs from the amorphous state in

ethyl-benzene films; possibly, the physical size or shape of the molecule inhibits the close packing necessary for crystallization and the formation of a well-defined CBDOS. On the other hand, considerable change in the surface work function is seen: the current onset decreases from approximately −0.0 eV at 26 K to −0.3 eV at 70 K and returns to 0.0 eV at 140 K.

From these results, it is evident that the LEET spectra are sensitive to the geometrical structure of a film, as expected from the relationship shown in this section between the CBDOS and LEET features of rare gas solids[116,117,121] and in previous studies of long-chain alkanes.[36] *In fact, these results suggest that LEET spectroscopy can be used as a simple, convenient, and inexpensive method to qualitatively monitor structural changes in evaporated organic and molecular films*, as well as changes in work function of the metal substrate.

As a general rule, sufficiently thick (15−100 Å) disordered films exhibit LEET features in the collective regime, which are representative of the CBDOS. However, in thinner films and/or highly ordered films, QSEs could appear if the boundaries are well-defined.[27] Structure resulting from intramolecular electron resonances can also be seen, if these lead to strong electron energy losses to molecular vibrations. When the film is too thin, scattering by defects and energy losses to phonons and vibrations may not be sufficiently intense to redistribute electrons in random directions. Thus, a portion of the penetrating electrons are capable of conserving a specific momentum during their residence in the film, allowing constructive and destructive interferences of the electron wave to evolve between the film−vacuum and film−substrate boundaries.[28,39] These QSEs modulate the usual transmission features emerging from the bulk CBDOS. QSE features are indicated by vertical arrows in the LEET spectra[28] of three to six layers of Ar and CH_4 in Figure 10. This is further shown in Figures 11 and 12 for thin films of N_2 and CO molecular solids. The dc and DD (i.e., doubly differentiated) LEET spectra[35] recorded with 10 ML films appear at the bottom and above, respectively, in both figures. The rise near 7 eV in N_2 and 5 eV in CO in the dc curves is due to energy-loss electrons that increase the transmitted current. The vibronic structure is clearly apparent in the DD curves shown in the upper portion of Figures 11 and 12. The broad features below the onset of electronic excitation at 6 eV for CO and 6.5 eV for N_2 belong to the collective regime. The set of peaks from 2.4 to about 5 eV, especially in nitrogen, is composed of oscillations whose amplitude and number depend critically on the thickness. Such variations are indicative of QSE, but they could be mixed with CBDOS features. The first set of peaks in N_2 between 0 and 2.4 eV is characterized by fairly evenly spaced (280 meV) peaks, which are present even at submonolayer coverage. HREEL measurements on thin[122,123] and thick[107,122,124] films of N_2 on a metallic substrate have indicated that the vibrational cross section is large in the 0.8−2 eV energy range, owing to the presence of a $^2\Pi_g$ shape resonance.[125,126] Furthermore, more refined measurements[122,124] for levels where $\upsilon = 1$, 2, and 3 indicate that this resonance produces oscillatory structures or peaks in the excitation functions of these states, which originate from vibrational motion of the temporary N_2^- ion. These peaks are spaced by the same energy as those in Figure 11 lying below 2.4 eV. Collectively, these facts suggest that the structure observed between 0.8 and 2.4 eV in N_2 is caused by vibrational energy losses, which are strongly enhanced

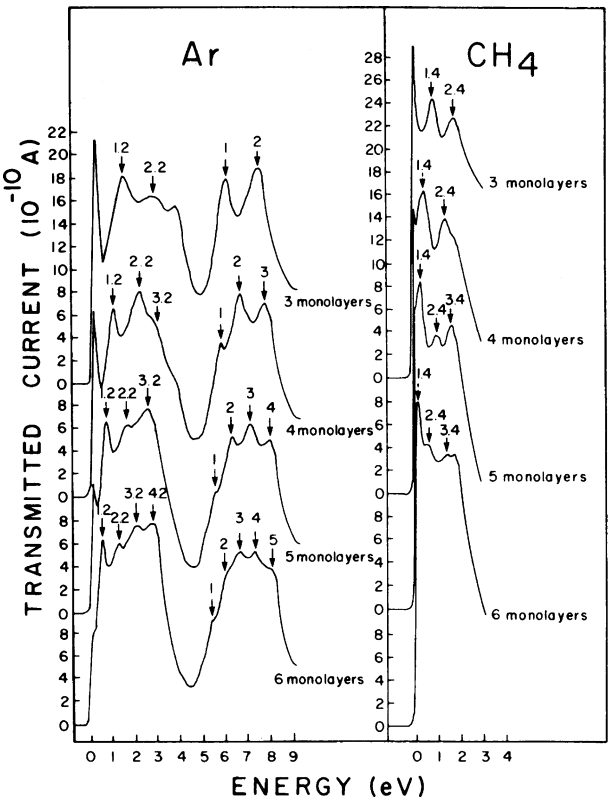

Figure 10. Transmitted current in Ar and CH_4 as a function of incident electron energy for film thicknesses ranging from 3 to 6 monolayers (ML). The arrows point to the interference structure caused by multiple reflections of the electron waves between the film−vacuum and film−substrate interfaces. The numbers refer to the assigned values of the interference order. Reprinted with permission from ref 28 (http://link.aps.org/abstract/PRL/v55/p545). Copyright 1985 by the American Physical Society.

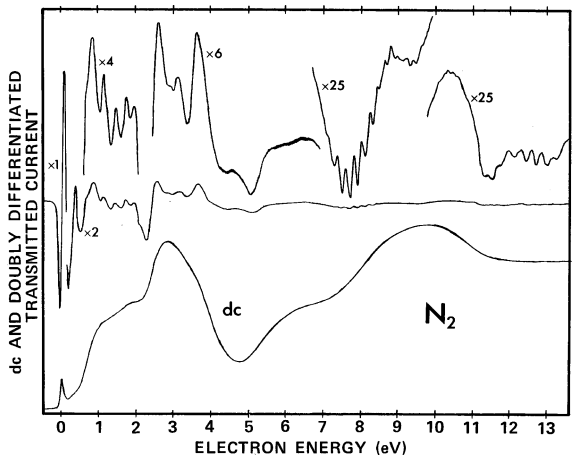

Figure 11. LEET spectrum (bottom curve) of N_2 on Pt, together with its doubly differentiated (DD) spectrum (middle curve). Various sections of the DD-LEET spectrum have been amplified by a factor indicated near every section (top curves). Reprinted with permission from ref 35 (http://link.aps.org/abstract/PRA/v35/p607). Copyright 1987 by the American Physical Society.

by the formation of the same N_2^- state. Similarly, the structure below 2 eV in CO originates from transient formation of a $^2\Pi$ state of CO^-.[127]

5. Measurements of Electronic Excitation near Threshold in Molecular Solids by LEET

When the excitonic channels become accessible in a molecular film, quasielastic scattering competes directly with

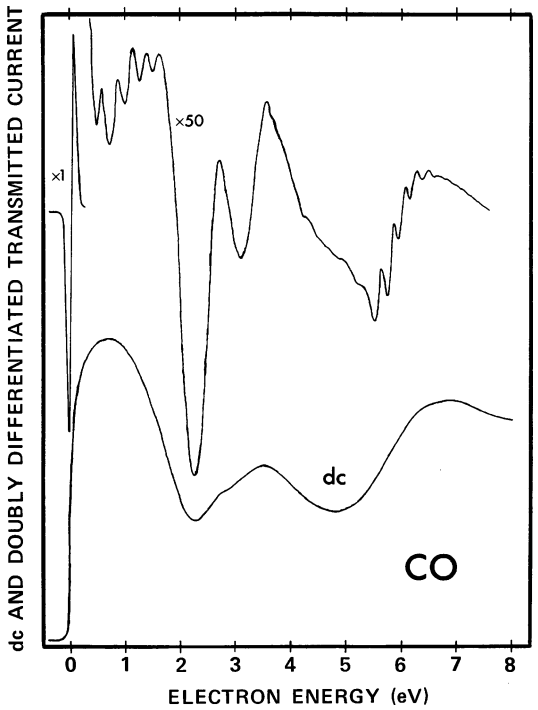

Figure 12. LEET spectrum (bottom curve) of CO on Pt, together with its DD-LEET spectrum (top curve). Reprinted with permission from ref 35 (http://link.aps.org/abstract/PRA/v35/p607). Copyright 1987 by the American Physical Society.

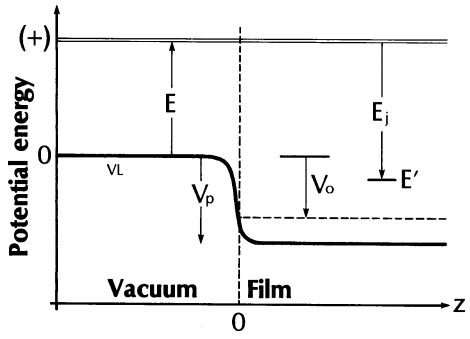

Figure 13. Simplified potential-energy-level diagram for an electron of energy E entering a solid film from vacuum along the z direction. The horizontal double line and the heavy line represent the total electron energy and the potential energy with respect to VL, respectively. The vertical dashed line denotes the film−vacuum interface. V_p is the potential energy due to electronic polarization of the dielectric by the negative charge of the electron. After exciting a level of energy E_j, the electron reaches a final energy, E'. The dashed horizontal line represents the energy of the lowest conduction level, V_0, of the solid.

electronic transitions and loses its preponderance, and coherence in the electron waves is eliminated. As a result, LEET features above the electronic excitation threshold represent the inelastic cross section near the energy threshold for such an excitation (i.e., for electrons to lose essentially all of their energies). The mechanism producing LEET structures related to electronic transitions may be explained by referring to a simplified potential energy level diagram for an electron of energy E entering a solid film in the z direction from a vacuum. Such a diagram is shown in Figure 13, where the heavy line and horizontal double line represent the potential energy with respect to VL and the total electron energy, respectively. The vertical broken line at $z = 0$ denotes the film−vacuum interface. The value V_p is the average potential energy resulting from electronic polarization of the dielectric by the negative charge of the electron. The dotted horizontal line represents the energy of the lowest conduction level, V_0, of the solid. After having produced an electronic transition of energy E_j, the electron is found at *a lower level in the film "conduction band"* with energy $E' = E - E_j$. An inelastic event can occur only if a free energy level is available to accommodate the lower-energy electron. Hence, at the electronic excitation threshold $E' = V_0 = E - E_j$. This simple relationship between V_0, E and E_j shows how LEET can be used to measure V_0 by measuring the onset energy of the inelastic regime. More specifically, the probability amplitude P_j of an electronic transition j for an electron of initial energy E, a wave vector k, a final energy E', and a wave vector k' is represented by

$$P_j \propto (1/h)\langle A',E',k'|T|A,E,k\rangle, \qquad (5)$$

where A and A' are quantum numbers specifying the density of state of the medium before and after the inelastic event. T indicates a transition operator that cannot be expressed in simple form[128] except in the Born approximation,[129] where expression 5 reduces to the Fermi golden rule.[115] This, however, is not expected to be valid for electronic transitions near the threshold, since in this case the final wave vector k' is necessarily quite different from the initial wave vector k.[129] As shown in eq 5, the sensitivity of LEET to electronic energy levels of solids involves a convolution of a joint density-of-states: one at energy E' and another one at energy E.

According to this mechanism, referred to as the "V_0 mechanism", excitation of a bound electron in a film to an unoccupied state by an incoming electron scatters the electron to a lower-energy state. Near the electronic excitation threshold, such inelastically scattered electrons "fall" to the lowest "conduction" level of the film. Their transmission probability becomes unity when the band edge (i.e., V_0) lies below VL. As the electron energy is increased, excitation of the same transition produces electrons of correspondingly increasing energy, up to a point, where they have nonzero probability of escaping in a vacuum. From then on, the transmitted current usually progressively diminishes unless another electronic transition with a comparable magnitude becomes energetically possible. Thus, as the electron energy is swept across the energy of an electronic transition, an increase in transmission is followed by a tailing decrease. However, the situation is different for films with a positive V_0, but because of the image potential of the metal, backscattering to a vacuum of near 0 eV electrons in the film is small. Therefore, even for films having a positive V_0 energy loss, electrons increase the transmitted current near the electronic excitation threshold. The V_0 mechanism has been considered by many authors[6,31,35,36,41,45−47,96,130] and is introduced in calculations via refraction (i.e., Snell's law).[33,44,45,90] A systematic and quantitative assessment of its validity and influence on the magnitude and shape of inelastic features has been given by Marsolais et al.[35]

The V_0 mechanism reveals the presence of several energy loss features in the DD LEET spectra of N_2 and CO, shown in Figures 11 and 12, respectively. In the DD LEET spectra of N_2, at least two series of peaks are observed below 10 eV: one barely visible series below 7.2 eV and one series of strong and narrow peaks above 7.2 eV. The position of the steepest slope on the low-energy side of each peak closely matches the vibronic progressions of the A $^3\Sigma_u^+$ and the B

$^3\Pi_g$ electronic states of N_2, respectively. The relative amplitudes are also quite consistent with those seen in HREEL spectra,[35] even though the incident energy is slightly different. A striking similarity is observed between these results and those obtained with the trapped-electron method in the gas phase,[131] which also measures the cross section for electronic excitation near threshold. The peaks above 8.5 eV also match the a $^1\Pi_g$ state, but there is apparently no trace of the Δ states. The spectra in Figure 11 also consist of at least two other series. The C $^3\Pi_u$ progression in N_2 can be made to coincide with the minima in the observed structure, but above 11.8 eV, the progression of peaks cannot be attributed to any known electronic state of N_2. Their width (140 MeV) is somewhat larger than that of the other peaks. They probably originate from optically forbidden states having a strong cross section near the threshold, which are hidden by Rydberg states present in the gas-phase HREEL spectra of N_2[127] but absent in the solid phase.

The DD LEET spectra for CO in Figure 12 show a single series of peaks spaced by about 200 meV, starting at 5.8 eV. It is easily attributed to the X $^1\Sigma^+ \rightarrow$ a $^3\Pi$ transition, provided that the electron energy inside the film is increased by a few 100 meV to compensate for induced polarization. Thus, these results and the sharp and narrow structure observed in the DD spectra provide evidence for the occurrence of large cross sections near the threshold for exciting the a $^3\Pi$ state of condensed CO molecules.

6. Determination of Quasi-Elastic and Inelastic Mean Free Paths (MFPs) by LEET

Since in LEET spectroscopy one measures the total current passing through a thin film sample, this technique provides a way to determine absolute values for electron MFPs. However, in LEET, electrons suffer multiple collisions before their collection at the metal substrate, so extraction of MFPs from such spectra must involve a mathematical description of electron scattering within the film and at its interfaces. Thus, considerable effort has been made to unravel the effects of multiple scattering from LEET spectra, and to this end, several theoretical approaches have been developed. MFP determined from LEET spectroscopy can be compared with measurements obtained from the attenuation of substrate photoelectrons injected into a molecular solid following UV irradiation of a metal substrate.[4,55] The results obtained with this photoinjection technique[63] before 1991 have been reviewed by Marsolais, Cartier, and Pfluger.[4]

The earliest attempts to unravel the scattering sequence within films[45] employed a unidimensional or "two-stream" model to approximate the multiple reflections, toward and away from the metal substrate, of an injected electron within a Xe film. This model was used, with other simplifying assumptions, to obtain an expression for the transmitted current as a function of film thickness, elastic MFP, and the reflection coefficients of the vacuum−film and film−metal interfaces. The elastic MFP was obtained by fitting the behavior of the transmitted current as a function of film thickness, at numerous energies in the 0−10 eV range[45] Subsequently, a 3D electron transport model was developed that combined a semianalytical simulation of the transport of an excess electron in a film's conduction band with a random sampling of the temporal succession of the various elastic and inelastic scattering events.[82,90,132,133] The injected electron was assumed to scatter isotropically from imperfections within the film and to transfer its energy via quasi-elastic and inelastic collisions. In a crude approximation, the total electron MFP was assumed to be constant over the 0−10 eV energy range studied, and the effective mass of the electron was taken to be the free electron mass. The MFP associated with elastic and specific inelastic processes was then adjusted until an agreement emerged between the theoretical and experimental LEET curves. This type of analysis was employed to study benzene[90,132] and tryptophan.[82,133] For benzene, the total inelastic MFP "λ_T" was found to be ~0.8 nm, whereas for tryptophan it was in the range $0.34 < \lambda_T < 0.85$ nm. Additionally, the inelastic MFP in the region of electronic excitation "λ_{elec}", which represents the mean distance traveled by the electron before such excitation occurs, was calculated for tryptophan as $9.0 < \lambda_{elec} < 280$ nm. Despite the simplifying assumption of a constant total MFP, these results today still represent the best available information concerning electron MFPs in these two compounds.

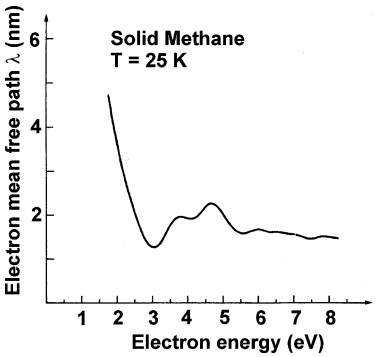

Figure 14. Energy dependence of the electron scattering mean free path (MFP) for solid methane in the quasi-elastic scattering region at 25 K. Reprinted from ref 89a, Copyright 1985, with permission from Elsevier.

During the same period of time, a quantum mechanical approach was developed.[33] The transmission of electrons through a dielectric film was considered a two-step process. Electrons were envisaged as being initially scattered at the film−vacuum interface, where they penetrated the film's surface potential barrier to an extent proportional to the CBDOS. Subsequently, electrons propagated in Bloch states in all possible directions in a manner similar to a single MFP. An analytical formula was obtained for the transmitted current as a function of film thickness, which allowed both the CBDOS and the MFP to be obtained in the collective regime. The model was used to obtain MFPs for electrons in solid Xe,[33,88] N_2,[89] and methane[89] films. Those for methane are reproduced as an example in Figure 14.

A considerable advance in the analysis of LEET spectra and the measurement of electron MFPs was the development of a general 3D probabilistic model of electron transport.[91] The new model took into account the partial reflection of electrons at boundaries and included the effects of multiple quasi-elastic[91] and inelastic scattering.[134] The validity of assumptions regarding the isotropic electron scattering within a solid was investigated in a series of Monte Carlo calculations.[90] The complete model has been applied to electron transmission through N_2,[134] copper phthalocyanines,[98,99] and rare gas[135,136] films and revealed an almost inversely proportional relationship between total MFP and the CBDOS. Subsequently, the assumptions underlying this probabilistic model were investigated and an accurate model was developed using elementary diffusion theory.[137] The results for

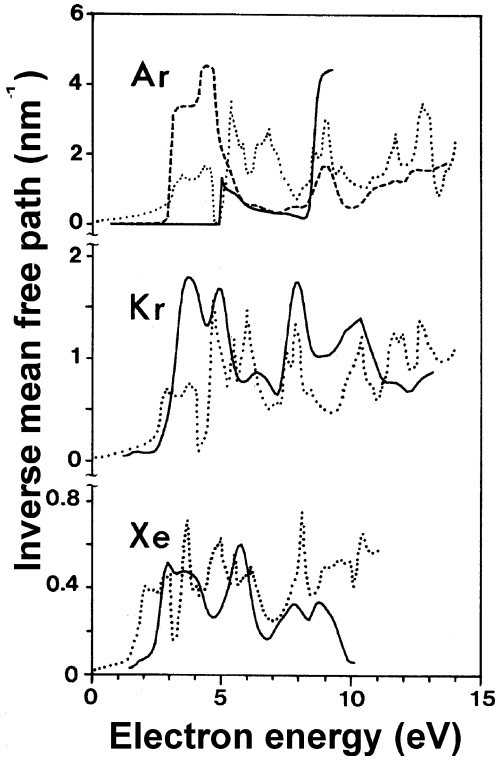

Figure 15. Plots of the inverse of the total (elastic and inelastic) MFP (i.e., the total scattering frequency per unit path length) for Ar, Kr, and Xe. Dotted lines represent the CBDOS. Reprinted from ref 136, Copyright 1992, with permission from Elsevier.

rare gas solid films, shown in Figure 15, illustrate the relationship between total MFP and the CBDOS.[136]

7. Measurement of Surface Charges by LEET

With LEET spectroscopy, it is also possible to measure the number of charges that have accumulated near the surface of a dielectric film, resulting from the electron bombardment.[48] When electrons from the monochromator, shown in Figure 2, have just enough energy to enter the multilayer film, deposited on the substrate R, a sharp rise, termed the "injection curve" (IC), is seen in the LEET spectrum. The IC for an uncharged film is represented by the upper curve of Figure 16. When the same film is charged at the surface by the electron beam, the IC is shifted by ΔV to a higher accelerating potential (bottom curve, Figure 16), since the incoming electrons must then possess additional kinetic energy to overcome the negative potential barrier. The IC is also broadened due to the effect of space charge and the current density distribution. Such measurements are usually performed in conjunction with all types of thin film low-energy electron experiments to ascertain that the target does not charge significantly during the time of the experiment. However, if the film is purposely allowed to charge at its surface by a significant potential ΔV, this can be related to the trapping cross section by treating the dielectric film as a charged capacitor.[48] The potential barrier ΔV is related to the charge density $n(t)$, which has accumulated after bombardment time t, by the relations

$$\Delta V(t) = n(t)d/\epsilon \quad \text{and}$$
$$\sigma(t) = n_0\{1 - \exp(\beta t)\}; \quad \beta = (\sigma_{CT}J_0/e) \qquad (6)$$

where, ϵ is the permittivity of the film, d its thickness, n_0 the initial ($t = 0$) trap density, σ_{CT} the trapping cross section, J_0 the incident current density, and e the unit charge. In the limit $t \rightarrow 0$, a charging coefficient $A_s = d\Delta V/dt$, directly proportional to the trapping cross section, can be expressed as

$$d\Delta V/dt|_{t=0} = \{(dn_0J_0)/(\epsilon e)\}\sigma_{CT} = A_s \qquad (7)$$

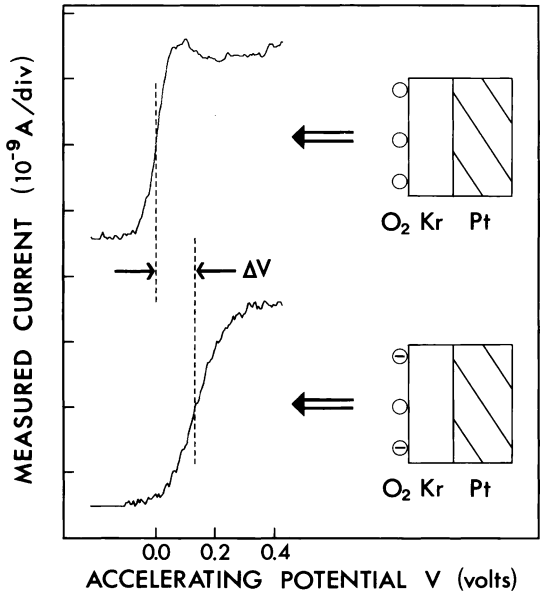

Figure 16. Current transmitted through an uncharged (top) and a charged (bottom) Kr film covered with 0.1 ML of O_2 as a function of the accelerating potential V of the incident electron beam.

The experiment is performed as follows. A multilayer film that does not charge under electron impact is first deposited on a metal substrate. Afterward, submonolayer amounts of molecules, which act as electron traps (i.e., the density of surface molecules becomes the trap density), are condensed on top of the multilayer film. The IC of a freshly deposited surface-doped film is first recorded rapidly (e.g., during 0.1 s) to avoid any significant charging. The film is then bombarded at a given voltage V applied between the monochromator and the film for a much longer period (e.g., 25 s) with the same incident current (i.e., $I_0 \approx 5 \times 10^{-9}$ A). Afterward, the IC is again rapidly recorded, and the shift ΔV is determined by comparison with the initial IC. Such a cycle can be repeated many times on the same film with the same V to obtain the time dependence of the process. To measure the electron energy dependence, a new film has to be deposited for each data point. However, if film charging can be reduced to the beam resolution, measurements as a function of electron energy can be made on a single film without appreciably affecting the total energy resolution of the experiment.

The charge at the surface is created by electron capture below VL or by the formation of stable anions, which often do not possess sufficient kinetic energy to escape the image potential they induce in the dielectric and in the metal substrate. Thus, for total electron and ion capture, σ_{CT} becomes an absolute trapping cross section. Desorption of anions induced by electrons of energy below 10 eV can be verified by mass spectrometry. If no anion desorption occurs, then σ_{CT} represents the absolute cross section for stable anion formation at the film surface. Under the best conditions, the smallest ΔV that can be measured in these experiments is 0.5 mV, which allows the measurement of *absolute charge*

trapping cross sections as small as 10^{-19} cm^2. The absolute energy scale, which is accurate to approximately ±0.1 eV (monochromator ±50 meV, charging ±50 meV), is calibrated by taking as 0 eV the point of the steepest slope of the IC (i.e., taking VL as 0 eV). Analysis of errors, including those associated with the preparation of the target film, suggests a total error of ±50% for the absolute values of the measured cross sections.

Electron trapping cross sections have been measured for numerous simple molecules adsorbed in submonolayer quantities onto the surface of a dielectric film.[138−149] Electrons can be trapped via several mechanisms including dissociative electron attachment (DEA). This is a two-step process well-known from gas-phase studies,[150] in which an electron attaches to a molecule to form a transient negative ion, which subsequently dissociates into a neutral and a stable anionic fragment.

Two further mechanisms have been observed to trap electronic charge in thin films: *intermolecular* and *resonance stabilization* (IMS and RS, respectively). In the latter process, electron attachment to a molecule produces an anion in a vibrationally excited state, which is then de-excited by energy exchange with neighboring molecules. When the initial anion ground state lies below the band edge or the lowest conduction level of the dielectric, then the additional electron may become permanently trapped at the molecular site. In this case, a permanent anion is formed (e.g., the case of O_2[138]). When electron trapping can be attributed to DEA or RS processes alone, σ_{CT} is equivalent to a cross section for stable anion formation. IMS refers to the trapping of very low energy electrons by an aggregate of molecules typically unable to do so in the monomeric form. In this sense, the process is similar to solvation, which usually requires the organization of polar molecules to form a suitable trap. Incident electrons are initially temporarily captured into pre-existing traps formed during condensation. By losing energy to phonon modes of the molecular solid in hopping from one trap to another, they become permanently trapped at an intermolecular site. IMS has been observed for water clusters condensed on Kr and Xe surfaces at cryogenic temperatures[140] and in pure water films.[151] Both IMS and RS occur at incident electron energies below 1 eV. Since DEA can, in some systems, occur at similar energies, it is not always easy to identify which process is responsible for charge accumulation. Fortunately, further information can usually be obtained from measurements of the desorbed yield of anions from similar films and from a comparison with gas-phase data.

In Figure 17, we show a few examples of the dependence of σ_{CT} on incident electron energy, for the chloromethanes, for example, CCl_4, $CHCl_3$, CH_2Cl_2, and CH_3Cl.[143−145] In the gas phase, Cl^- production via DEA to these molecules is observed over the 0−10 eV energy range and is expected to be responsible for the CT features reported in the figure.[143−145] Features appearing in the data at energies greater than 5 eV can be correlated to an anion desorption signal from similar films induced by a 5−10 eV electron impact.[152] The absence of such a signal at low incident electron energies implies that the cross section measurements below ~2 eV in Figure 17 represent the absolute cross section for DEA. At higher energies, however, σ_{CT} must be considered a minimum cross section for the DEA process as some Cl^-, representing an unknown fraction of the total yield.[141] Such measurements made it possible to study the effects of the solid-phase

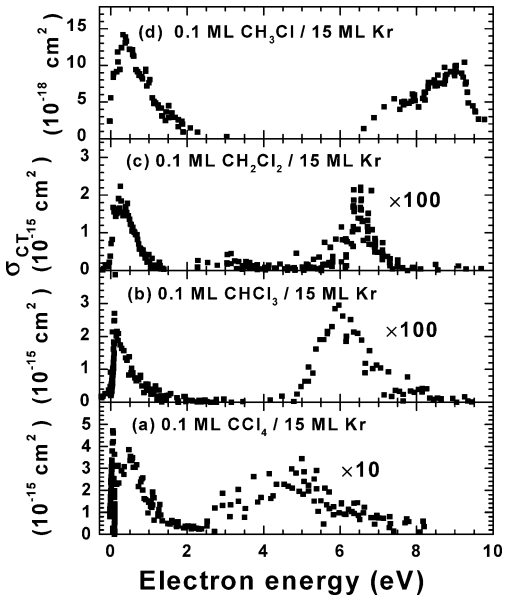

Figure 17. The dependence on incident electron energy of the charge trapping cross section, σ_{CT}, for isolated chloromethane molecules condensed onto the surface of a multilayer Kr film. Data were obtained for 0.1 ML of the indicated molecule deposited onto a 15 ML thick Kr film. Panels a−c reused with permission from A. D. Bass, J. Ganache, P. Ayotte, and L. Sanche, *Journal of Chemical Physics*, *104*, 4258 (1996). Copyright 1996, American Institute of Physics. Panel d reused with permission from P. Ayotte, J. Ganache, A. D. Bass, I. I. Fabrikant, and L. Sanche, *Journal of Chemical Physics*, *106*, 749 (1997). Copyright 1997, American Institute of Physics.

environment on DEA by comparing the absolute cross section in the gas and condensed phases. Usually, an enhancement in cross section relative to that of the corresponding gas-phase process was observed. The cross sections of analogous processes can vary greatly between the gas and condensed phase, differing by as much as a factor of 10^6 for CH_3Cl.[143]

Electron trapping processes (e.g., DEA, RS, and IMS) are greatly affected by a change in local environment. This sensitivity to the local environment was investigated by varying the thickness of the supporting Kr film in charge-trapping experiments for CH_3Cl,[143,145] CH_3Br,[145] and $CFCl_3$.[149] As illustrated in Figure 18 for the example of CH_3Cl, σ_{CT} initially increases as the Kr film thickness is reduced from 20 ML, reaching a maximum value at 5 ML. Below this thickness, the cross section is observed to decrease. A shift to lower the energy of the maximum in σ_{CT} is simultaneously accompanied by a decrease of film thickness, which is depicted at the bottom of the figure. A further shift to a lower energy and enhancement of σ_{CT} are observed when electron-trapping molecules are covered by layers of Kr.[147,105] Besides chloro- and fluoromethanes, absolute values of σ_{CT} were reported for condensed CF_4, O_2, CO_2, N_2O, and H_2O.

The decrease in σ_{CT} with increasing Kr thickness reported in the previous paragraph can be generally explained by a change in the polarization-induced interaction between the environment and the temporary trapping anion molecule. This interaction modifies the energy of the transient anion responsible for DEA with respect to that of the ground state parent molecule. Consequently, the branching ratio between electron emission from the anion and electron stabilization on a molecular fragment is modified, thus affecting the cross section of the latter process. More specifically, the increase σ_{CT} from 20 ML to about 3 ML is essentially due to the

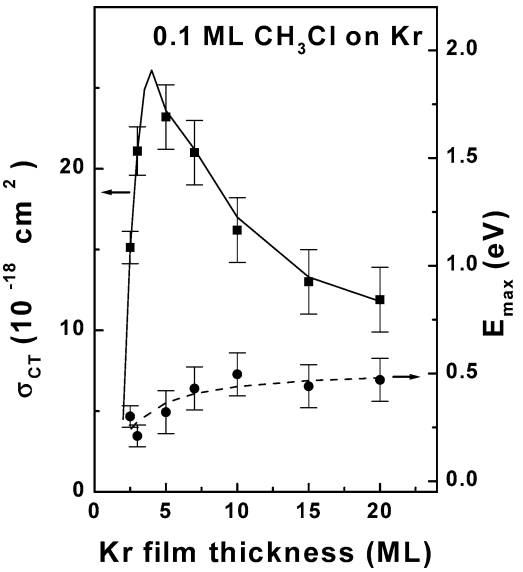

Figure 18. Variation of maximum σ_{CT} with Kr film thickness for low-energy electrons incident on 0.1 ML of CH_3Cl deposited on the surface of Kr films (—). Also shown is the variation in energy of the maximum in σ_{CT} with Kr film thickness (– – –). Reprinted with permission from ref 143 (http://link.aps.org/abstract/PRL/v75/p3568). Copyright 1995 by the American Physical Society.

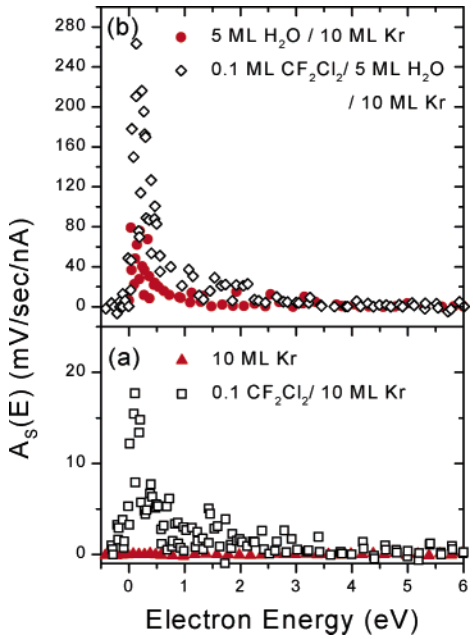

Figure 19. Charging coefficient, A_s, as a function of electron energy for (a) 10 ML Kr condensed onto a Pt substrate (▲) and 0.1 ML CF_2Cl_2 on 10 ML Kr (□) and (b) 5 ML H_2O on 10 ML Kr (●) and 0.1 ML CF_2Cl_2 on 5 ML H_2O on 10 ML Kr (◇). Reprinted with permission from ref 172 (http://link.aps.org/abstract/PRB/v63/e153403). Copyright 2001 by the American Physical Society.

increased stabilization of the transient anion by the image charge induced in the metal and Kr layer, whereas below 3 ML, the steep decrease is caused chiefly by a reduction of the lifetime of the anion owing to the possibility of electron transfer to the metal substrate.

More recently, absolute σ_{CT} measurements have been applied to problems of atmospheric interest, particularly to the problem of ozone depletion. The presence of ionizing radiation in the upper regions of the earth's atmosphere and the realization that "atmospheric" chemistry can occur on the surface of ice and dust particles have led to studies of the interactions of LEE with molecular solids of ozone,[153] HCl,[154] and halogen-containing organic compounds[120,141,143−145,147,148,155−169] in an effort to shed new light on the problem of ozone depletion.

In a series of experiments, Lu and Madey[170,171] found that the F^- and Cl^- yields produced by the impact of 250 eV electrons on CF_2Cl_2 adsorbed on a Ru surface were enhanced by several orders of magnitude, when the CF_2Cl_2 was coadsorbed with polar molecules such as H_2O and NH_3. Subsequent charge-trapping measurements by Lu and Sanche[172] also displayed an enhancement in stable anion formation at electron impact energies near 0 eV, implying that secondary electrons having near-thermal energies were responsible for the enhancement observed by Lu and Madey. Figure 19a shows the charging coefficient $A_s(E_i)$, which is directly proportional to σ_{CT}, for 10 ML of Kr deposited on Pt foil (solid triangles) and that for 0.1 ML of CF_2Cl_2 deposited on the Kr surface (open squares). These results can be compared with those in Figure 19b for 5 ML of H_2O on 10 ML of Kr (solid circles) and for 0.1 ML of CF_2Cl_2 on 5 ML of H_2O on Kr (open diamonds). In contrast to pure Kr films, which do not trap electrons, both H_2O- and CF_2Cl_2-covered films show significant charging. Those for CF_2Cl_2 correspond to a maximum trapping cross section of 1.4×10^{-15} cm^2 [172] near 0 eV, attributed to charge stabilization as Cl^-, via the DEA reaction $CF_2Cl_2 + e(\sim 0\ eV) \rightarrow CF_2Cl_2^- \rightarrow CF_2Cl + Cl^-$ [173] and here enhanced by approximately an order of magnitude with respect to gas-phase DEA by the effects of surface polarization [e.g., ref 143]. However, when the same quantity of CF_2Cl_2 is deposited on H_2O, the charging coefficient per CF_2Cl_2 molecule at 0 eV increases by more than a factor of 10 to yield $\sigma_{CT} = 1.3 \times 10^{-14}$ cm^2. A further order of magnitude enhancement in σ_{CT} is observed for CF_2Cl_2 on NH_3.[172]

It has been argued,[172] by analogy with the case of molecules adsorbed on glassy *n*-hexane,[120] that this enhancement is due to electron transfer to CF_2Cl_2 of an electron previously captured in a precursor state of the solvated electron in the water layer, which lies at or just below the vacuum level,[171,172] and its subsequent molecular dissociation via DEA. Similar results have been reported for HCl adsorbed on water ice.[154] It has been proposed that in polar stratospheric clouds the enhanced DEA to CF_2Cl_2 via electron transfer from precursor-solvated states in ice[172] may explain the correlation between cosmic ray activity (which would generate secondary low-energy electrons in ice) and atmospheric ozone loss.[174]

8. LEPET through Organized Organic Thin Films (OOTFs)

In recent years, studies were performed on electron transmission through organized organic thin films (OOTFs). These films can be formed either using the self-assembly technique or via the Langmuir−Blodgett method. In the OOTF, periodicity in the potential exists both in the direction perpendicular to the layer's plane (*z*-axis) and in the directions parallel to the layer (*x*,*y*). In the *z* direction, the periodicity is a result of almost all the chemical functionalities being identical to the CH_2 groups. The situation in the *xy* plane is different, however; here the periodicity results from having the molecules adsorbed in an organized layer. If the interaction between the molecules is weak (van der Waals forces), then no band structure can be observed for the highest occupied

molecular orbital (HOMO). However, when an additional electron is injected into the film the situation changes.

While in a bulk solid the addition of an electron does not affect the interaction between subunits, in the OOTFs the additional electron makes all the difference. This can be understood as follows. In bulk solids, the total Hamiltonian describing the system is given by

$$H = \sum h_n + \sum V_{nm} \tag{8}$$

where h_n is the Hamiltonian of each subunit in the solid and V_{nm} is the interaction between the subunits. The bandwidth is characterized by V_{nm}, which in typical nonmolecular solids is large. When an additional electron is added to the system, it induces a new interaction between the subunits, V'_{nm}, and the Hamiltonian is now given by

$$H = \sum_n h_n + \sum_{n \neq m} V_{nm} + \sum_{n \neq m} V'_{nm} \tag{9}$$

Since in a typical solid $V_{nm} > V'_{nm}$, the addition of an electron does not significantly change the interaction between the subunits and therefore does not affect the band structure. In OOTFs, the interaction between the subunits is weak, and therefore no band structure can be observed in the spectroscopy of the neutral system. This means that V_{nm} is small, on the order of van der Waals interaction, and therefore the band is very narrow. However, when an electron is added to the system, the interaction due to the additional electron is much larger than that when all the molecules are neutral and therefore, $V'_{nm} \gg V_{nm}$.This means that the addition of an electron significantly increases the coupling between the subunits. This "electron-induced coupling" results from the low dimensionality of the system, which forces the electron to be localized in one dimension (perpendicular to the surface-*z* direction), while being delocalized in the other two dimensions. Hence, in the presence of an additional electron and because the electron cannot be delocalized on the direction, the charge density is high enough to alter significantly the interaction among the molecules. Therefore, significant "band structure" exists *only* in the presence of an additional electron.

The importance of the two-dimensional periodicity on the transmission properties is shown in Figure 20, which presents the transmission probability of electrons as a function of the photoelectron energy for layers made by the Langmuir−Blodget method from cadmium salts of arachidic [Cdar, $(CH_3(CH_2)_{18}COO^-)_2Cd^{2+}$] or brassidic [Cdbr, $(CH_3(CH_2)_7CH{=}CH(CH_2)_{11}COO^-)_2Cd^{+2}$] acids or a mixture of both,[175] for three (Figure 20A) and nine (Figure 20B) layers. As is clearly evident, the electron transmission through the mixed layers is much less efficient than that through the Cdar or Cdbr layers themselves. Moreover, the spectrum for the mixed layers is much closer to the relaxed type, as shown in Figure 1. Namely, because of the destruction of the order in the system, the electrons are not transmitted any more through well-defined bands and the transmission efficiency drops.

Some word of caution, however, is needed regarding this point. The notion of electronic bands is of course related to the electronic structure of ordered bulk solids, and applying it to thin films is, in principle, questionable. Indeed, it is sufficient to associate high transmission probabilities with states of the excess electron in the films that are extended on the scale of the film's thickness. In fact, numerical results[176] suggest that the correspondence with the band structure of the bulk material is substantial even for very thin films.

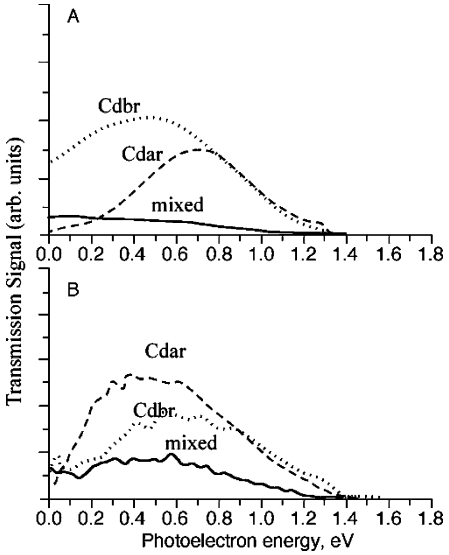

Figure 20. The photoelectron energy distribution for electrons transmitted through layers of Cdar (− − −), Cdbr (•••), and mixed monolayers (—) for three (A) and nine (B) layers. Reused with permission from A. Kadyshevitch, S. P. Ananthavel, and R. Naanan, *Journal of Chemical Physics*, *107*, 1288 (1997). Copyright 1997, American Institute of Physics.

The results presented in this section indicate that "band conduction", or transmission through electronic states that are extended, is the cause of the efficient electron transmission through amphiphiles. It also explains the observation that electrons are better conducted through all-trans amphiphilic chains than through chains containing some gauche bonds; that is, when the chains are in an all-trans configuration, the layer is ordered and the electronic wave functions in the band are delocalized. The formation of the gauche bonds requires introducing disorder, which increases scattering and reflection and, when sufficiently pronounced, localizes the electronic wave function.

9. Angular Distribution of Photoejected Electrons in LEPET

As previously mentioned, one may view the LEPET and LEET spectroscopy techniques as complementary in an interesting way: in LEET and HREEL spectroscopies, one controls the energy and direction of the incident electron beam, whereas in LEPET one resolves the energy and direction of the transmitted signal. In both types of experiments, electron transmission is examined through thin films at positive (relative to vacuum) electron energies. However, there is a possibility to also control, to some extent, the momentum of both the incident and the transmitted electrons in LEPET experiments. Hence, direct information on the transmission through the organic film as a function of the incident and scattered angles can be obtained.

The control of the momentum of the incident electrons is achieved by changing the laser−surface incident angle. The dependence of the photoelectron angular distribution on the laser−surface angle has been addressed both experimentally[177−180] and theoretically.[181,182] Although the theory and the experiments do not agree in all details, some basic principles emerge. It was found, for example, that for large

angles between the surface normal and the laser, the electron distribution also peaks at large angles but typically is smaller than the laser incident angle. As the incident angle of the laser relative to the surface normal becomes smaller, the peak of the electron distribution moves toward the surface normal; for example, when the laser−surface normal angle is 20°, the electron distribution peaks at about 5°.[178,181]

In these experiments, two setups are used. The first one is a modified photofragment imaging system described in detail elsewhere.[183] In brief, a uniform electric field generated by two parallel plate electrodes is used to accelerate photoelectrons toward a position-sensitive imaging detector located ~45 cm from the acceleration field. The OOTFs are mounted on the repeller electrode such that their surfaces are flush to each other and biased at the same voltage, typically −3 to −5 kV. The extractor electrode is grounded. Both the acceleration and the field-free region toward the detector are shielded from the Earth's magnetic field using two concentric tubes of μ-metal. Photoelectron images appearing on the detector's phosphorus screen are recorded using a slow-scan CCD camera. The size of each pixel is about 0.08 mm; therefore, the solid angle per pixel is 3×10^{-8} sr. The excitation laser is either a frequency-doubled Nd:YAG-pumped system or an ArF (193 nm) excimer laser. The laser is linearly polarized along a direction perpendicular to the surface normal, whereas the excimer laser is unpolarized. The pressure in the chamber during these experiments is 1×10^{-7} mbar.

In the second system, the experiments are performed in an UHV chamber pumped to below 10^{-8} mbar. Glass slides coated with gold, either bare or covered with OOTFs, are attached to a grounded holder and inserted into the chamber. An Nd:YAG-pumped dye laser with frequency mixing is used to eject photoelectrons from the substrate. A laser beam with a wavelength of 225 nm and a flux of about 50 nJ/mm^2 is introduced into the chamber in a horizontal direction through a quartz window. The photoemitted electrons are detected by a multisphere plate or multichannel-based detectors, which are placed parallel to the sample at a distance that can be changed from 10 to 75 mm. The detector is positively biased to 113 V relative to the grounded sample. The back anode of the detector is divided into seven vertical parallel strips. The width of each strip is 4 mm. By analyzing the signal from each anode separately, we are able to extract the angular distribution of the photoemitted electrons. The organic films are made from cadmium salt of stearic acid [CdSt, $(CH_3(CH_2)_{16}COO^-)_2Cd^{2+}$] using a Langmuir−Blodgett (LB) trough.

A strong dependence of the photoelectrons' angular distribution on the laser impinging angle has been found. It was observed that electrons are ejected mainly in the plane defined by the laser impinging and reflection angles, namely, in the *XZ* plane. Since the photon energy is very close to the surface work function, the energy distribution of the electrons is narrow and therefore the observed images can easily be converted to angular distribution in the following way:

$$\alpha = \frac{\pi}{2} - \arccos\left(\frac{x}{x_{max}}\right) \qquad (10)$$

where α is the angle in radians between the initial velocity of the emitted electron and surface normal, x is the distance between the electron position on the detector and the time-of-flight axis of the machine, and x_{max} is the maximum value of x, which corresponds to an electron being ejected at 90°.

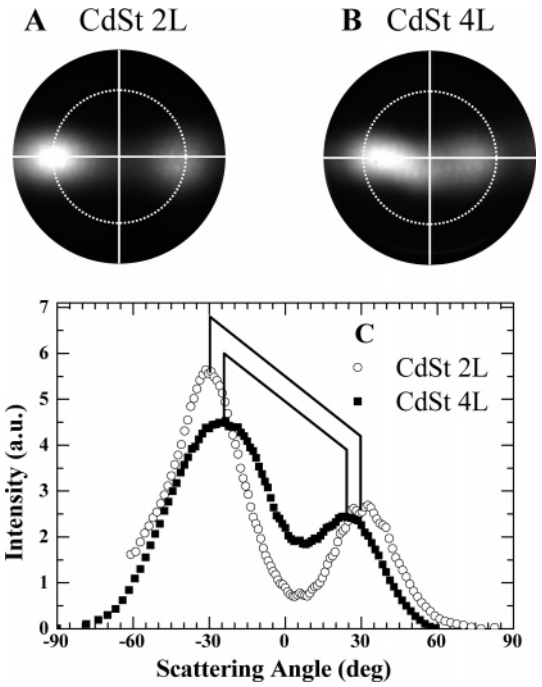

Figure 21. The images obtained for a gold surface coated with two (A) and four (B) layers of CdSt and (C) the angular distributions derived from the images. The laser-impinging angle is 88°. Reprinted from ref 184, Copyright 2000, with permission from Elsevier.

Figure 21 shows the images obtained for a gold surface coated with two and four layers of CdSt (panels A and B, respectively).[184] In Figure 21C, the angular distributions derived from the images are shown. Clearly, the angular distribution peaks move closer to the surface normal when the surface coverage changes from two layers to four layers. The sharper angular distribution, observed for the four layers sample, is consistent with the fact that four-layer systems are known to be better ordered than films with fewer than three layers.[80] In fact, LB films of Cdst are crystalline-like at room temperature for films that contain more than three layers.[185] By monitoring the ratio between the intensities corresponding to the CH_2 and CH_3 vibrations in the IR spectrum, we were able to ascertain that indeed the multilayer film is more ordered than the two-layered one. Hence, we observed a clear correlation between the order in the film and the selectivity in the transmission probability as a function of the $\bar{k}$ vector of the incident electrons.

The results of the imaging experiments are consistent with those obtained using the angle-resolved time-of-flight experiments. Figure 22A shows the displacement of the photoelectrons' signal from the center of the multichannel detector in the second experimental setup for bare gold surface and for gold coated with four layers of Cdst. The center of the detector corresponds to the normal scattering angle. The distance between the sample and the detector is 75 mm and the laser-impinging angle is 60° relative to the surface normal. In this case, the angular distribution of the photoelectrons emitted from the bare surface peaks at normal to the surface, and the distribution is very broad. When the surface is coated with four layers of Cdst, the photoelectrons' distribution narrows significantly. Figure 22B presents the transmission probability obtained by dividing the distribution obtained with the covered surface by the distribution of the

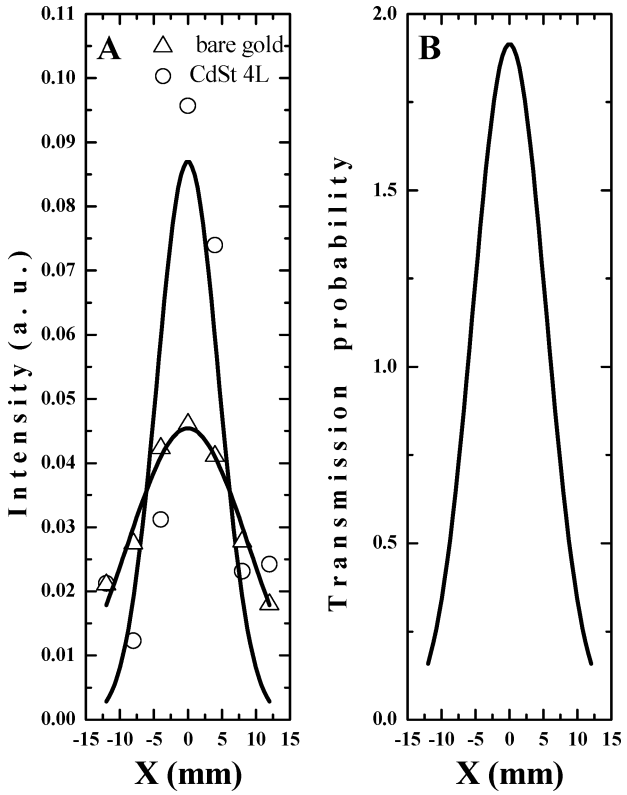

Figure 22. (A) The displacement of photoelectron signals from the center of the detector, as measured by the second experimental setup for a bare gold surface and for gold coated with four layers of CdSt. Zero displacement corresponds to a normal scattering angle. Here the laser impinging angle was 60° relative to the surface normal. (B) The transmission probability obtained by dividing the distribution obtained with the covered surface by the distribution of the bare surface. Reprinted from ref 184, Copyright 2000, with permission from Elsevier.

bare surface. The enhancement of the signal in the normal direction indicates a "channeling" effect, namely, that electrons are emitted from the metal surface at angles different from normal, which are scattered by the OOTF toward the normal direction. This type of process is well-known for high-energy particles scattering through crystals.[186]

The results presented here show that the angular distribution of low-energy photoelectrons ejected from a gold substrate *is not isotropic* and depends strongly on the laser-impinging angle. The photoelectrons emitted are confined into the plane defined by the laser impinging and reflection directions. It is also demonstrated that the transmission of electrons through OOTFs depends strongly on the electrons' entrance angle. In general, the electron transmission is by far more efficient along the chains of the organic molecules than in any other direction.

10. Electron Transmission through DNA Monolayers

Many of the mutagenic or lethal effects of ionization radiation can be attributed to secondary electrons that are created within 10^{-15} s along radiation tracks and spurs and have kinetic energies below 20 eV.[187,188] Experimental[189] and theoretical[190] studies indicate that electrons with subionization energies play an important role in inducing damage to DNA.[191] But, the detailed mechanism underlying electron−DNA interaction is difficult to address experimentally *in vivo*, where many parameters affect the electron−DNA interaction and the electron energy is not well-defined. However, using LEPET spectroscopy, it has been possible to investigate the interaction of LEEs of a limited energy range with monolayers of single- (ss) and double-stranded (ds) DNA oligomers chemisorbed on a gold surface. By methodical variation of the bases in the oligomers, the effect of each base on the interaction with electrons could be determined, as well as the difference between single and double strands. Furthermore, the binding energy of the captured electrons could also be determined.[192] In brief, the work described in this section was to determine the structural and chemical elements in the DNA that govern the initial electron-capturing process, by studying electron transmission through organized adsorbed layers of DNA.

Past findings hint that guanine (G) bases act as "DNA protectors". For example, G-rich telomeres found at the ends of chromosomes[193] were recently shown to increase the resistance of DNA to ionizing radiation.[194] It is also well-established that guanine is the most easily oxidized nucleotide;[195,196] hence a positive charge localizes on the G bases. It has also been demonstrated that positive charges can be transported over long distances in DNA through multistep hopping between G bases.[197−200] The putative role of G bases as protectors of the genome from electrons with kinetic energies greater than the ionization energy of the bases seems to result from their ability to easily form cations.[201,202] Hence, LEPET studies specifically focused on the role of the guanine bases in the interaction of the DNA oligomers with the electrons.

Self-assembled DNA monolayers were prepared according to the standard procedure,[203,204] that is, by depositing 3′ thiolated 15-mers of DNA on clean gold substrates. Fifteen-base single-stranded, disulfide (S−S)-protected oligonucleotides were suspended in 0.4 M, pH 7.2, phosphate buffer. The clean Au slide was covered uniformly with the oligomer solution.

In order to form layers of dsDNA, 3′ thiolated ssDNA was hybridized *ex situ* with its complementary nonthiolated DNA oligomer by combining equal amounts of the two oligomers. Complete hybridization was determined by non-denaturing gel analysis. The hybridized ds oligomers were then deposited using the same protocol as that for ssDNA oligomers.

Figure 23 shows the different DNA oligomers and their corresponding abbreviations used in the study. The monolayers were characterized by atomic force microscopy, contact angle measurements, and ellipsometry. The sample preparation and characterization are described in detail in ref 192.

Several control experiments were performed in order to verify the validity of the electron transmission results. The first experiment checked whether the UV light, used for ejecting the electrons, damages the adsorbed DNA layer. Radiolabeled DNA oligomers were exposed in solution to 193-nm light with an energy density (100 nJ/cm^2) 50 times larger and an exposure time (14 s) 10^6 times longer than were used in the experiment (2 nJ/cm^2 and 20 μs). By gel electrophoresis analysis, no single-stranded breaks could be detected in the DNA.

In addition, by monitoring the electron signal as a function of the laser intensity, one can verify that the electrons ejected from the gold are indeed produced by a single photon. The results indicate that there is a linear dependence of the electron signal on the laser flux.

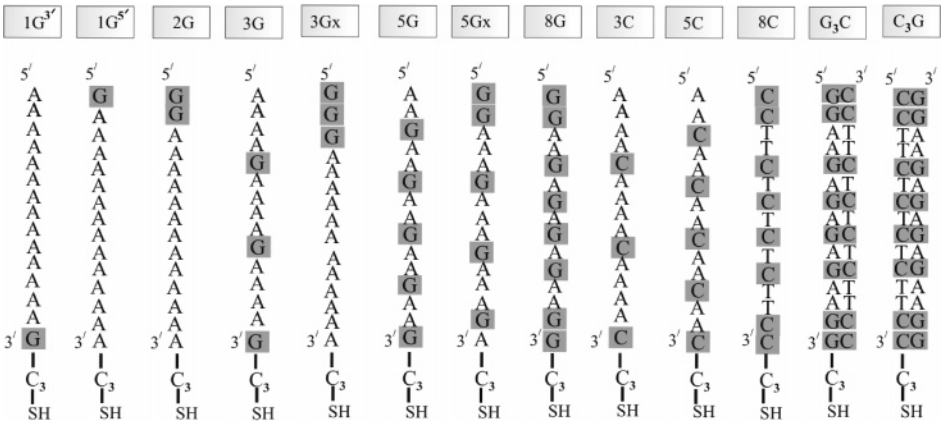

Figure 23. The different DNA oligomers used in the experiment and their abbreviations. In oligomers $3G_x$ and $5G_x$, the guanine bases are clustered together. G_3C and C_3G are double-stranded oligomers bound to the substrate through a propyl-thiol group attached to either the G or C single-strand oligomer, respectively. Reprinted with permission from ref 192. Copyright 2005 by The National Academy of Sciences of the U.S.A.

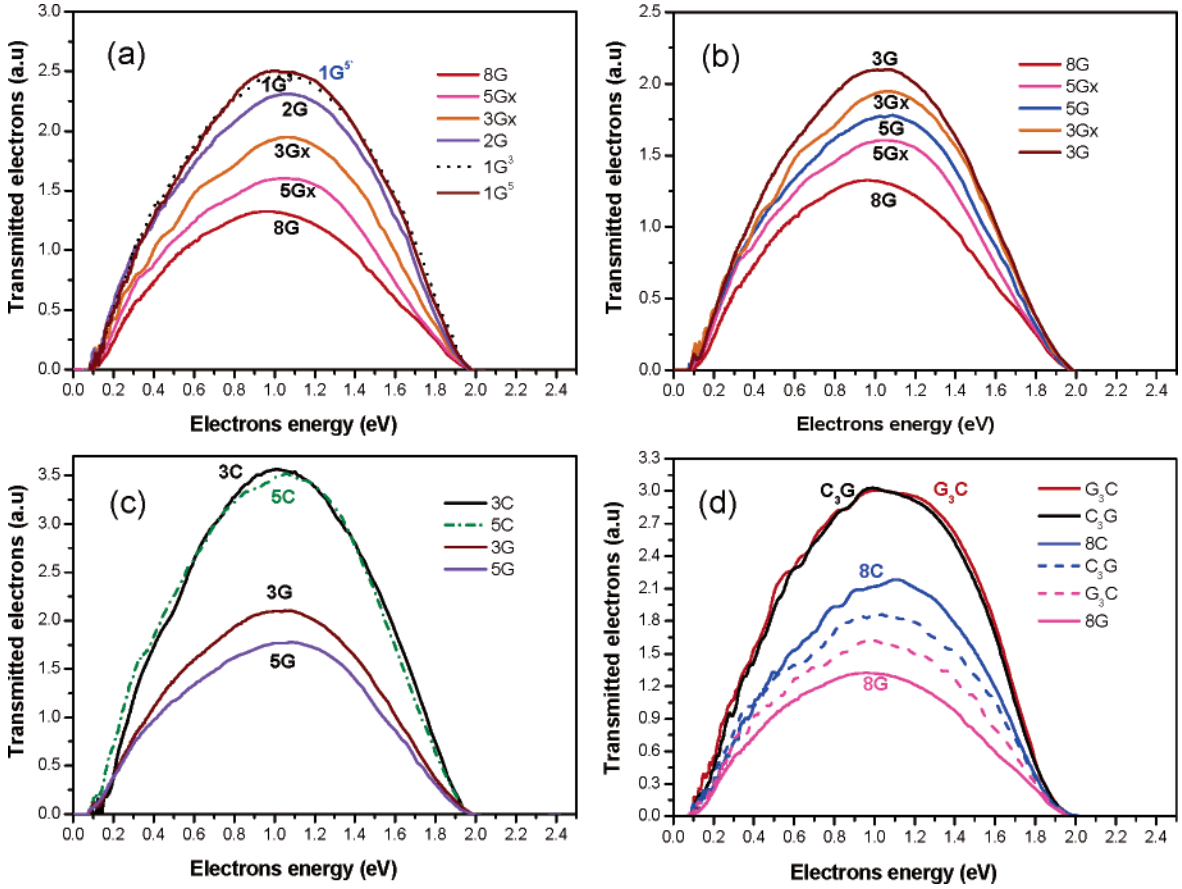

Figure 24. (a) The kinetic energy spectra of photoelectrons transmitted through monolayers made of single-stranded DNA oligomers containing 15 bases with various numbers of guanine, the rest being adenine bases. The photon energy is 6.4 eV. The abbreviations of the strand sequences are given in Figure 23. (b) The effect of clustering of the G bases on the transmission signal. When the G bases are clustered together ($3G_x$, $5G_x$), the transmission yield is reduced compared with the oligomers where the guanine is separated by adenine bases. (c) The kinetic energy spectra of photoelectrons transmitted through monolayers made of various oligomers (see Figure 23 for the assignment). The transmission through layers made of the 3C and 5C oligomers are compared with 3G and 5G. (d) Kinetic energy spectra of photoelectrons transmitted through layers made of double-stranded DNA (red and black solid lines). For a comparison, the transmission through layers made of single-stranded DNA is shown (8C, 8G). The curves with the dashed lines correspond to the spectra obtained after washing the ds samples with pure water to induce denaturation. Reprinted with permission from ref 192. Copyright 2005 by The National Academy of Sciences of the U.S.A.

Finally, in order to probe the effect of the salt (and therefore the counterion) on our measurements, we prepared DNA monolayers on gold from an ethyl alcohol solution instead of water, and we performed electron transmission experiments. Interestingly, the results were identical to those obtained for monolayers made from aqueous solutions of DNA.

Figure 24 shows the electron signal vs energy for photoelectrons ejected from the gold substrate and transmitted through monolayers composed of the different ssDNA oligomers. The data in Figure 24a indicate that the electron transmission intensity decreases as the fraction of G bases in the DNA oligomer increases. The same transmission

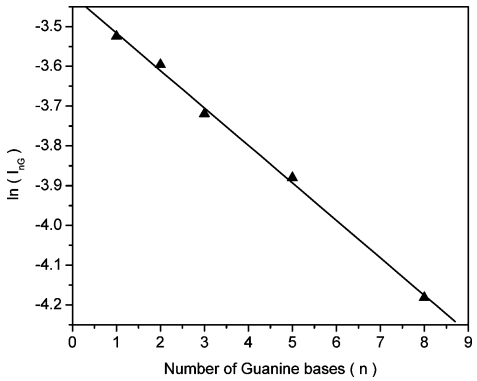

Figure 25. The measured integrated transmission yield (I_{nG}) as a function of the number of guanine (G) bases in the DNA oligomers. The straight line indicates that $I_{nG} = I_{Au}\, e^{-Nn(\sigma_G - \sigma_A)}$ with $\sigma_G - \sigma_A = (67 \pm 24) \times 10^{-16}$ cm^2. Reprinted with permission from ref 192. Copyright 2005 by The National Academy of Sciences of the U.S.A.

efficiency was obtained whether the single G base was positioned at the 5′ end or 3′ end of the DNA oligomer (farther [seq. $1G^5$] or closer [seq. $1G^3$] to the surface, respectively). The transmission yield is lower when the G bases are clustered together [oligomers $3G_x$ and $5G_x$] (Figure 24b) than when they are separated by an adenine base [3G and 5G]. In addition, the transmission efficiency was found to be much higher for monolayers made of DNA oligomers consisting of the C and A bases rather than the G and A bases (Figure 24c). The transmission is more efficient through layers made of double-stranded DNA than with the single-stranded ones (Figure 24d). Importantly, the capturing by layers made of dsDNA is about 2.3 times less efficient than the capturing by a layer made of ss GA-rich oligomers, and 1.5 times less efficient than the capturing by layers made of ss CT-rich oligomers

To confirm the effect of the double strand, after measuring the transmission, the samples were washed extensively with water in order to denature the double-stranded DNA. Following the washing, the transmission efficiency decreased (dashed lines in Figure 24d), as expected from a double-stranded DNA that had been converted to mainly single-stranded oligomers.

The above qualitative description can become quantitative if one calculates the energy-integrated photoelectron signal ($\int I(E)\, dE$). I_{nG}, the integrated electron transmission signal (Figure 25) obtained for the nG oligomer, can therefore be calculated by $I_{nG} = I_{Au}[1 - P]$, where P is the integrated capturing probability of the electrons by the layer, which is given by $(I_{Au} - I_{nG})/I_{Au}$, and I_{Au} is the signal from a bare gold substrate. Since the shape of the spectra does not change as a function of the number of guanine bases, one can conclude that within the studied energy range of the electrons, the capturing probability is energy-independent.

The integrated intensity of the transmitted electrons can be represented by $I_{nG} = I_{Au}\, e^{-Nn(\sigma_G - \sigma_A)}$, where N is the number of adsorbed molecules per unit area and σ_G and σ_A are the scattering cross sections for electrons scattered from a G and an A base, respectively. Figure 25 shows that indeed a plot of $\ln(I_{nG})$ versus n produces a good approximation to a straight line. Three sets of experiments were performed, and the slopes indicate that the cross section for electron scattering from a guanine base is larger by about 67×10^{-16} cm^2 than the cross section of adenine:

$$\sigma_G - \sigma_A = (67 \pm 24) \times 10^{-16}\ \text{cm}^2$$

This difference in cross section is large but not unreasonable for an electron interacting with a molecule possessing a large dipole moment. Boudaiffa et al.[205] measured the cross section for 10−50 eV electron damage to DNA by creating DNA strand breaks and obtained values of up to 30×10^{-16} cm^2. Since the electrons' captured cross section is expected to be higher than that for the actual breaking of the DNA, the results obtained here are consistent with those in ref 205.

To explore the state of the captured electrons on the adsorbed layer, we conducted two-photon photoemission (TPPE) studies.[206,207] In these experiments, electrons are excited in the metal substrate with photon energy below the substrate's work function. Some of these electrons are transferred to the LUMO of the adsorbed layer. A second photon is used to eject these electrons from the LUMO to the vacuum, and their kinetic energy, E_k, is measured. The kinetic energy of the electrons ejected by the TPPE process is therefore related to their binding energy to the layer, E_b, so that $E_k = h\nu - E_b$ when $h\nu$ is the photon energy, which in the present study is 3.55 eV.

Figure 26 presents the TPPE spectra observed for DNA layers composed of different oligomers. The TPPE signal depends on the transition probability (k_T) of the electrons from the metal to the layer and on the lifetime of the electrons residing on the LUMO. This lifetime depends on the relaxation rate of the electrons back to the metal (k_R). Hence, an intense TPPE signal means either that the layer captured very efficiently the excited electrons (k_T is high) or that the lifetime of the electron in the LUMO is very long, allowing for a high transient population. On the other hand, the electron transmission intensity depends only on the capturing probability by the layer and not in any way on the LUMO lifetime. When comparing the results from two different experiments (electron transmission and TPPE), one sees that the calculated capturing probability from the electron transmission experiment matches closely the normalized electron capture probability calculated from the TPPE experiment (see Table 1). The normalized capturing probability was calculated assuming that the difference in the TPPE signal depends only on the capturing probability of the electrons. Hence, the ratios between the integrated TPPE signals provide the ratio between the capturing probabilities. Figure 26a shows that in the case of single-stranded oligomers, the TPPE signal increases with an increasing number of G bases in the oligomer. More specifically, it is inversely proportional to the transmission signal in Figure 24a and proportional to the capturing probability. In addition, when the guanine bases are clustered together (oligomers $3G_x$ and $5G_x$), the capturing probability increases (Figure 26b). This inverse correlation between the transmission signal and the TPPE signal for layers made of single-stranded oligomers means that both results are controlled by the capturing probability of electrons by the layer. When the capturing probability is high, the transmission signal is weak, whereas the TPPE signal is strong and vice versa. Hence, the TPPE signal is controlled by the transmission probability from the metal to the DNA layer, k_T, and it shows no effect due to the variation of the lifetime of the LUMO states. Hence, the lifetime of the LUMO must be about the same for all oligomers. This indicates that the LUMO may be the same for all single-stranded oligomers.

The TPPE studies clearly show that for layers made from single-stranded DNA, the energy distribution of the ejected

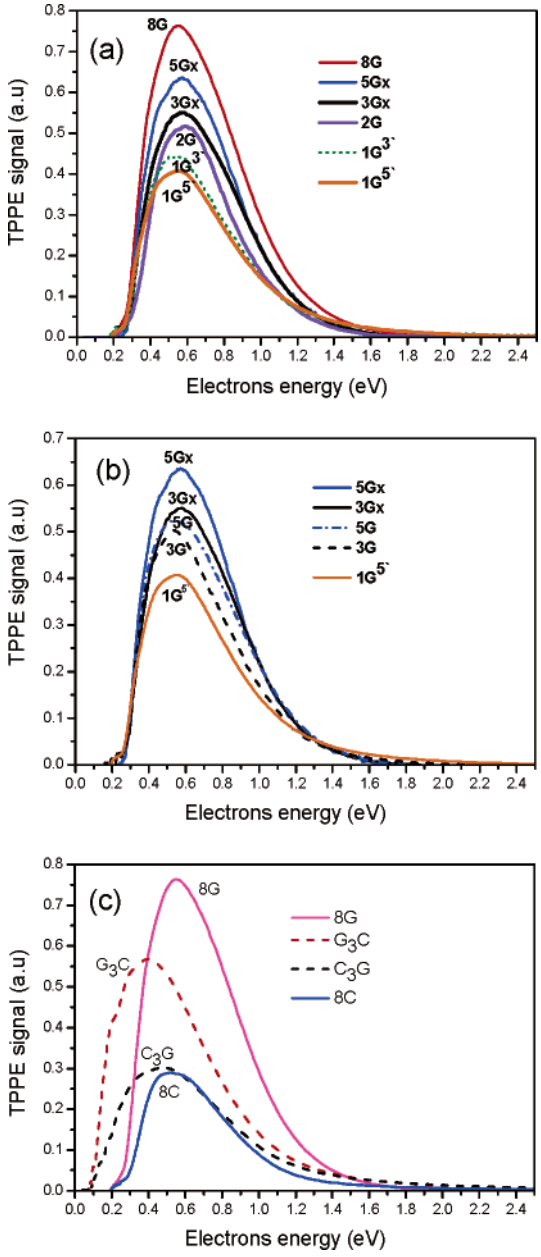

Figure 26. Kinetic energy spectra of electrons ejected by a two-photon photoemission (TPPE) process. The photon energy is 3.55 eV. (a) The TPPE spectra obtained from monolayers made of single-stranded DNA oligomers containing 15 bases with various numbers of guanine, the rest being adenine bases. (b) TPPE spectra showing the effect on the electron transmission due to clustering of the guanine bases ($5G_x$ and $3G_x$) versus the bases being separated by adenine bases (5G, 3G). (c) TPPE spectra from layers made of double-stranded DNA (dashed lines) versus layers made from single-stranded oligomers. Note the shift in the peak of the TPPE spectra for the double-stranded layers compared with the single-stranded layers. Reprinted with permission from ref 192. Copyright 2005 by The National Academy of Sciences of the U.S.A.

electrons does not depend on the sequence, as can be seen by the similar shape and peak position. This is consistent with the conclusion that the nature of the LUMO is the same for all single-stranded oligomers, as indicated by the same lifetime. For the double-stranded oligomers, the TPPE signal (Figure 26c) is stronger than expected, based on the capturing probability derived from the transmission experiments, when compared with the transmission probabilities. This indicates that the difference between the TPPE spectra of the layers made from single- versus double-stranded oligomers is not due solely to the difference in the capturing probability but also depends on the lifetime of the electrons in the LUMO (low k_R); that is, the lifetime of the LUMO in the layers made from double-stranded DNA is longer than that in layers made from single strands. This conclusion is further supported by the shape of the TPPE spectra, which indicates that the electrons on the double-stranded layers are more strongly bound by about 0.2 eV compared with the electrons bound to the single-stranded layers.

Table 1. The Electron Capturing Probability

strand	1G(3)	1G(5)	2G	3G	$3G_x$	5G	$5G_x$	8G	5C	3C	G_3C	C_3G
capturing prob. % ± 2[a]	44	43	47	54	57	61	65	71	22	22	31	33
capturing prob. % ± 3[b]	44	46	51	51	58	57	64	81			66	39

[a] Obtained from electron transmission studies where the capturing probability is given by $(I_{Au} - I_{nG})/I_{Au}$; I_{Au} is the energy-integrated photoelectron signal obtained for bare gold, and I_{nG} is the integrated electron transmission signal (Figure 24) obtained for the nG oligomer. [b] The calculated capturing probability is based on the TPPE signal (Figure 26) and is normalized relative to the signal obtained for 1G(3) oligomer.

The results indicate that the number of G bases controls the capturing efficiency of slow electrons. The fact that clustering of guanine bases is more efficient in electron capturing than guanine imbedded in an adenine sequence indicates that it is not the adenine−guanine combination, rather than solely the guanine, that affects the capturing. In the past, it has been assumed that high capturing efficiency of a base can arise either from its high electron affinity or from negative-ion resonances at energies relevant to that of the transmission electrons. It is important to realize that most quantitative experiments performed so far on the electronic properties of DNA bases, like ionization potential and electron affinity, were performed mostly in the gas phase and rarely in the condensed phase.[208−214] In addition, a comparison of the theoretical and experimental results shows that the determination of electronic affinity values of the DNA bases is still a matter of controversy.[215] One does expect that when the base is attached to the sugar backbone in an oligomer, its electronic properties will vary. Hence these former experiments are of limited use in our case. Another difficulty is that electronic structure calculations were performed usually on a single base and at most on a base pair. Again, the validity of these results to our experiments is questionable. Overall, both former studies and present calculations have predicted very low electron affinities for guanine. Clearly, guanine is not distinct from the other bases in terms of its electron affinity.

The special role of guanine can arise either from the high electron capturing probability or from the ability of the electron, once captured, to lose energy quickly and be stabilized on the DNA. The dipole moment for the biologically relevant form of guanine (amino−oxo tautomer) is about 7 D,[216,217] which is three times larger than that of adenine (2.2 D) and almost twice as large as that of thymine. However, cytosine (amino−oxy tautomer) also has a high dipole moment, like guanine.[190,218] However guanine is distinct because of its low ionization potential.[198−200] It has been found recently that, at least in the form of self-assembled monolayer, most of the phosphate groups on the DNA are not charged, namely, they are protonated.[219] Hence, one may speculate that the explanation for the role of the guanine is as follows. The protonated phosphate group, with

its high electronegativity, attracts charge from the guanine making the guanine slightly positively charged and the phosphate negatively charged. Hence, clearly electrons will be attached very efficiently to the positive guanine. Guanine is unique because of its low ionization potential. Hence, this effect cannot be found for the other bases. It is important to realize that if the phosphate is not protonated, then because of it being negatively charged, it cannot attract more electrons from the guanine and the guanine is expected to remain neutral. The role of the guanine in the electron capturing clearly deserves further calculations and experiments.

The results presented here indicate that, once captured, the electron is not localized on one of the bases but instead is either on the sugar backbone or between the molecules in the monolayer in a nonlocalized state.[220] The recent observation that the phosphate is protonated[219] may support the conclusion that the captured electrons are localized on the most electronegative group, namely, on the protonated phosphate.

The low capturing yield by monolayers made of dsDNA oligomers may result simply from their better organization. Whereas monolayers made from ss oligomers are expected to form irregular layers due to their less rigid structure, the monolayers made of the dsDNA are more organized because of the rigid and regular structure of the double helix. Numerous studies show that, in general, the capturing of low-energy electrons by well-organized and regular monolayers of organic molecules is by far less efficient than in the case of irregular layers.[2] Hence, the difference obtained between the electron capturing yield by layers made of ss- and dsDNA is consistent with the difference in their organization. Interestingly, it is well-established that *in vivo*, close packing of DNA strands enhances their protection against radiation damage.[221,222] Despite the fact that the experiments were performed in a very different environment than under the *in vivo* conditions, the dsDNA layers most likely contain structural water[195] and therefore include all the basic building blocks of DNA in their *in vivo* environment. Their density is also similar to the one observed *in vivo*. Hence, our observation relating the organization of the DNA to the reduction of electron capturing suggests that a similar mechanism possibly exists in a biological environment.[223]

11. Spin-Dependent LEPET

Electron circular dichroism (ECD) measurements are historically prominent because of the discovery of parity violation in β-decay in 1956 and the subsequent theories of Vester and Ulbricht[224] on the origin of biological homochirality by the interaction of β-rays with primordial chiral molecules. In LEPET, measurements of ECD are performed by comparing the transmission intensity (I) of spin circular polarized ($P = \pm 1$) electrons. An asymmetry parameter is defined by

$$A = \frac{I(+P) - I(-P)}{I(+P) + I(-P)}$$

Accurate measurements of the asymmetry parameter A in the gas phase of camphor molecules[225] have shown that the model of Vester and Ulbricht cannot be supported by experiments. In particular, the results for energies below 10 eV show $|A| < 2 \times 10^{-5}$ for organic chiral molecules that do not contain heavy elements (e.g., with low-spin orbit parameters).

A substantially different result was obtained for ECD measurements on thin organic LB films of amino acids on gold substrates.[226] A partial polarization (15%) of the electrons was achieved by using circularly polarized light to eject the photoelectrons from the gold substrate.[227] The measured asymmetry parameter was a sizable fraction of a unit. This result is more than 4 orders of magnitude larger than the quoted results in gas phases for low Z chiral molecules. The huge asymmetry was confirmed, and more surprising observations were reported recently when spin-polarized electron transmission was measured for self-assembled monolayers of polyalanine on gold.[228,229]

Self-assembled monolayers (SAM) of either alkylthiols or L- or D-polyalanine polypeptides were investigated on a gold substrate. A cystine group has been added at the end of the polypeptide. The cystine, with its thiol group, served for binding the polyalanine to the gold substrate. When the cystine is connected either at the C- or N-terminal of the peptide, its dipole moment points either away or toward the substrate, respectively. Characterization and purification of polyalanine by high-pressure liquid chromatography was not possible due to the hydrophobic nature of this peptide. Instead, the powder from the synthesis was taken and characterized by two methods: matrix-assisted laser desorption−ionization mass spectrometry, which gave the mass of the polypeptide, and amino acid hydrolyses, which determine the type of amino acids in the polymer.

Three types of polyalanine monolayers were prepared, consisting either of L-alanine or D-alanine and having 16 and 22 amino acids, respectively, both connected to the surface at the C-terminal (hereafter referred to as LC and DC, respectively), and a monolayer of D-polyalanine consisting of 22 amino acids and connected to the surface at the N-terminal (DN). The structure and tilt angle of the films were determined by their Fourier transform infrared (FTIR) grazing angle. In helix peptides, the transition moment of the amide I band lies nearly parallel to the helix axis and that of amide II, perpendicular. Since transition moments, which are parallel to the gold surface, cannot be detected in grazing angle FTIR, the ratio between the intensities of the amide I band (1665 cm^{-1}) and the amide II band (1550 cm^{-1}) indicates the tilt angle of the molecules relative to the surface normal. The frequencies of amide I and amide II vibrations indicate that the molecules in the monolayers are indeed in the α helix form.

The thickness of the films was measured by ellipsommetry and was compared with the predicted thickness, as calculated by multiplying the length of each peptide by the cosine of the tilt angle as inferred from the grazing angle FTIR spectra.

Circular dichroism (CD) measurements were performed to verify the handedness of the layers. For the CD measurements, the polypeptides were deposited on 10 nm thick gold-coated quartz slides that are transparent to UV radiation down to 190 nm. The CD spectra indicate a right α helix form for the LC film and a left one for the DC film.

For the electron transmission studies, the samples were inserted into an UHV chamber at $<10^{-8}$ Torr. The polarized photoelectrons are ejected from the substrate by applying a laser beam at 248 or 193 nm. The laser beam is passed through a linear polarizer and a $\lambda/4$ plate to create either left- or right-handed circular polarized light. It has been established that right-handed circularly polarized light induces positive helicity in the photoelectrons ejected from the gold substrate and the reverse for the left-handed

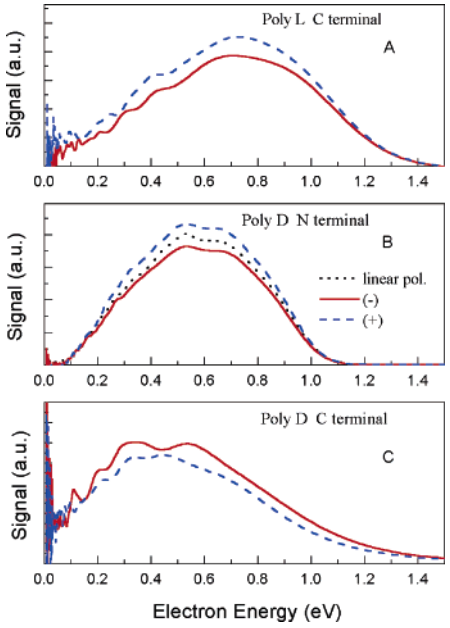

Figure 27. The energy distribution for photoelectrons ejected with a left (—) or right circular (— — —) polarized laser. The electrons are transmitted through films of L- and D-polyalanine both bound to the surface through the C-terminus (A and C, respectively) and through a film of D-polyalanine bound to the surface through the N-terminus (B). Reprinted with permission from ref 228. Copyright 2002 Wiley Interscience.

polarized light. Moreover, it is known that in the energy range of a few electronvolts the photoelectrons possess a polarization of about 15%.[227] After the electron passes through the organic layers, the its energy distribution is analyzed using a time-of-flight (TOF) spectrometer.

Results of electron transmission for the three different films, LC, DN, and DC, are shown in Figure 27. The 10% differences between the two circular polarizations correspond to about a 70% asymmetry parameter (due to the 15% partial polarization of the gold photoelectrons). As mentioned above, this result is many orders of magnitude larger than that in the gas phase. According to expectations, the LC and DC films have signs opposite to those of the asymmetry parameter for all measured energies. However, against expectations, the DN and DC films, which have the same molecular handedness, show opposite asymmetry of the spin-dependent electron transmission for all energies.

The voltage across the films was measured with a Kelvin probe and was found to be about +0.3, −0.3 and +0.3 V for the LC, DN, and DC films, respectively. These contact potential differences (CPD) are opposite and 2 orders of magnitude smaller than what is expected if the electric dipole moments of the free molecules are unchanged upon adsorption. These results can, however, be explained as due to a charge transfer of about one electron per molecule from the gold substrate to the LC and DC films or an opposite transfer (a hole per molecule) for the DN film.[230]

CPD measurements were carried out as a function of temperature for a LC film as well as the corresponding asymmetry measurements, which are shown in Figure 28. Upon cooling, the CPD drops from +0.3 V through 0 V at $T = 264$ K to −0.3 V. As expected, the asymmetry parameter jumps and changes its sign when the CPD changes its sign (Figure 28). Only at a very small region near $T = 264$ K does the asymmetry collapse to zero, and the electron spectrum dramatically changes its character. The spectrum

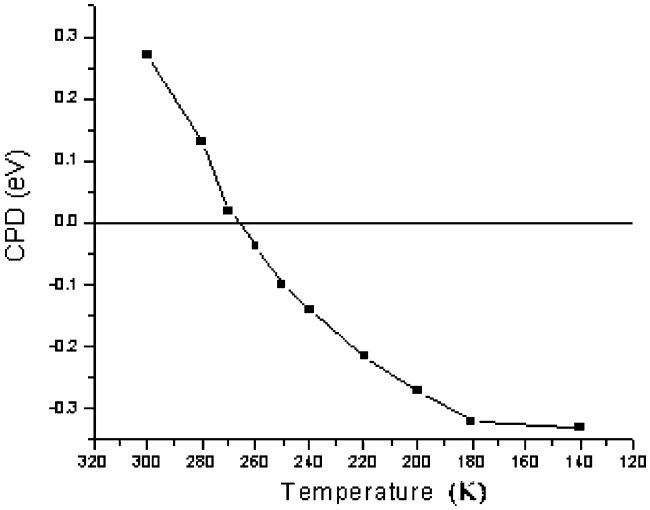

Figure 28. The change in the contact potential difference (CPD) as a function of temperature for gold substrate covered with a monolayer of L-polyalanine in α-helical form and bound to the surface through the carbon terminal. Reprinted with permission from ref 231 (http://link.aps.org/abstract/PRB/v68/e115418). Copyright 2003 by the American Physical Society.

at $T = 264$ K is believed to reflect an electron transmission through a homogeneous medium.[231] These results are consistent with a model that suggests an electron transfer from the gold to each molecule when the CPD is positive and a hole transfer when the CPD is negative. Only at a very small region near zero CPD is there no charge transfer and the asymmetry is also zero.

Two-photon photoelectron spectra were recorded from LC and DN films at a photon energy of 4.66 eV. Measurements were carried out at various temperatures and are shown in Figure 29. The photoelectron distribution from the LC film at room temperature is narrow (Figure 29B); thus only very low energy electrons are emitted. It shows a single photon dependence. When the sample is cooled down, the intensity of the photoelectron signal decreases until, at 260 K, a second broader peak starts to appear at appreciably higher energies. The intensity of this peak increases with a further decrease of the temperature. The increase and broadening of the energy distribution spectra of the LC film at low temperatures is an indication of the change occurring in the monolayer when cooled. As long as the CPD is positive (see Figure 28), only low-energy electrons are emitted with intensity that monotonically decreases with the CPD value. This is the region where a transferred electron resides on each molecule in the layer. An additional electron cannot bind to the molecule because it feels the repulsion from the already charged molecule. Therefore, only direct single-photon emission from the substrate is observed. Below $T = 260$ K, where the CPD is negative, the molecules are positively charged, and therefore an additional electron can reside in a metastable state. Subsequently a second photon can eject the electron from the metastable state to the vacuum. Hence, in this two-photon process, electrons are transferred by the first photon from the substrate to the layer and ejected to the vacuum by the second photon.

The reverse effect is observed for molecules connected to the substrate through their N-terminus (DN). The photoemission from the DN sample at room temperature is two-photon-dependent and decreases with decreasing temperature. Hence, we concluded that whereas the LC layer is negatively charged at room temperature and therefore cannot be charged

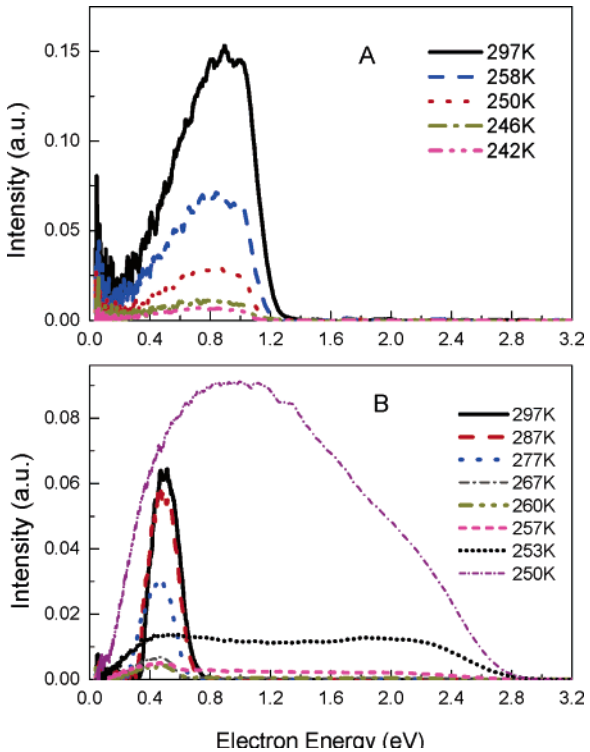

Figure 29. Two-photon photoelectron energy spectra as a function of temperature for the DN (A) and LC (B) layers of polyalanine. The photon energy used is 4.6 eV. At temperatures above 260 K in the DN layer (A) a two-photon process occurs, while a single-photon process occurs in the case of LC layer (B). When the temperature is lower than 260 K, no electrons are ejected from the substrate coated with DN and a two-photon process takes place in the case of the LC-coated surface and high-energy electrons are measured. Reprinted with permission from Figure 4 in ref 245. Copyright 2003 Israel Science Journals.

with an additional electron in a two-photon process, the DN sample is positively charged at the same temperature and hence a strong two-photon signal is observed. Upon cooling below 260 K, the charging on the layers reverses its sign, as indicated by the CPD signal, and therefore a two-photon process occurs on the LC layer, but the DN layer is now negatively charged and hence cannot be charged by an additional electron. Because of the high work function of the gold covered with the DN layer, a single photon signal is not observed either at this photon energy. The change in the charge is attributed to structural changes in the molecules. This effect was observed before,[232] but it is outside the scope of the present discussion.

The temperature-dependent studies prove that upon formation of the closed packed layer, charge is transferred between the substrate and the layer, consequently canceling the dipole−dipole interaction between the molecules. For example, in both the LC and DC layers, an electron is transferred from the metal to each molecule and that dramatically lowers the electrostatic energy within the layer.

In recent studies two new related effects were detected: (1) spin-selective electron transmission through monolayers made from chiral molecules, as reported here, and (2) the large magnetic moment measured for self-assembled monolayers.[233] In addition, it has been found that there is clear difference between monolayers made from ssDNA and those made from dsDNA. This difference exists despite the fact that both types of molecules are chiral.[234]

In trying to rationalize the observations, it is important to realize that chirality alone cannot explain spin selectivity and the same is true for the existence of the magnetic field itself. Recently several other studies reported "interface magnetism" similar to the one found in the above cases. This interface magnetism was observed for gold nanoparticles coated with organic molecules,[235,236] for thin HfO_2 layers on silicon and sapphire, and in irradiated carbon substrates.[237,238]

The explanation for the magnetism is based on the fact that upon organization of a SAM, charge is transferred, driven by the electrostatic repulsion between the aligned dipolar molecules in the SAM. It is important to realize that the charge transferred to each molecule is a fraction of a unit charge.[239] Thus, the extra charge is positioned on the monolayer in order to reduce the dipole moment of the molecules; this charge is squeezed on a two-dimensional net. Based on Hund's rule and as shown before, in each domain of the monolayer all the spins associated with these charges must be aligned parallel to each other. The charge squeezed between the two-dimensional network of molecules in the monolayer may possess large orbital magnetism. Hence, in each domain, except for the spin order parameter, there is an internal angular momentum order parameter that depends on the external magnetic field. However, if the adsorbed molecules are not chiral, then in each domain the spins can be oriented either toward or away from the substrate and the net magnetism with no magnetic field is therefore zero.

The situation is different, however, when the adsorbed molecules are chiral. Here the charge-transfer process, occurring upon organization, is directly related to the preferred direction of the angular momentum of the transferred electrons. Hence, upon electron transfer, the direction of the transient magnetic field is well-defined and energetically favors a unique direction for the spin order parameter. Thus, *for chiral molecules the spins of the transferred holes are aligned in the same direction for all domains*. The preferred direction of the spin depends on the handedness of the chiral molecule. The polarization of the spins can be detected by the magnetoresistance effect, namely, spin-dependent electron transmission. This effect is similar to the spin transmission preference observed in electron transmission through an ultrathin magnetic cobalt layer.[240] Indeed spin-selective electron transmission was observed only for chiral monolayers. For monolayers made from nonchiral alkylthiols, paramagnetism was measured,[241] but no spin selectivity in electron transmission could be observed.

The difference between the spin selectivity observed for single and double strands of DNA monolayers may be explained if one considers that dsDNA monolayers form well-organized layers and that the molecules themselves are rigid double helices with a right-handed helicity. In the case of ssDNA monolayers, the layer is much less organized and the molecules have no well-defined helix-type structure. Hence, the monolayers are not well-packed and therefore the electrostatic repulsion between the molecules can be reduced by their bending and reorientation rather than the charge transfer. For dsDNA monolayers, the only way the system can reduce the electrostatic repulsion is by charge transfer.

12. Summary

The study of electron transmission through thin organic films provides information unavailable from any other source on the electronic properties of the organic molecules as individuals and on the properties that emerge due to

interactions among the molecules in the film. These properties relate to many technological applications varying from the insulation of electrical lines[242] to radiation damage in biological tissues[243] and futuristic molecular electronic applications.[244]

The two methods described in the present review are complementary in nature. In LEET studies, a monochromatic electron beam hits an adsorbed molecular layer from the vacuum side; the transmission is monitored via the current generated in the conducting substrate. The same experimental setup can be used to study reflection. Both transmission and reflection are studied as functions of the incident electron energy, substrate type, and characteristics of the molecular layer. In the LEPET experiments, photoelectrons are ejected from a conductive substrate and are transmitted through the organic film to the vacuum side. Here the signal is the (angle- and velocity-resolved) transmitted electron flux as a function of incident photon energy, molecular film thickness, adsorbate, and substrate types and temperature.

The two methods, LEET and LEPET, are sensitive to the electronic states in the films that are above the vacuum level. Namely, unbound electron−molecule states. Only when the electrons lose some of their initial kinetic energy can they be trapped in states below the vacuum level. Hence, these techniques may also provide indirectly insight into the bound electronic states. Relevant information on these lower energy regimes may also be obtained by monitoring current vs voltage in contacts made of two metal electrodes separated by a molecular spacer or in scanning tunneling microscopy, STM, where a surface scan of the current versus bias voltage can be measured as a function of film thickness (i.e., tip−substrate separation). An older technique, inelastic tunneling spectroscopy, is commonly used to obtain information on nuclear motion in the barrier by observing their effect on the electron-tunneling process.

In the near future, it is expected that electron transmission studies will be used to obtain details on the properties of electronic excited films and on films composed from hybrid structures like nanoparticles self-assembled with organic molecules or biomolecules. These films are becoming important building blocks in biotechnology and electronics. Because of the sensitivity and depth of information that can be obtained on very thin layers, electron transmission studies have the potential to become an important tool for studies in the fast expanding field of research on thin films.

13. List of Abbreviations Used in the Text

CBDOS	conduction band density of states
CD	circular dichroism
Cdar	cadmium salts of arachidic acid
CPD	contact potential difference
DD-LEET	doubly differentiated LEET
DC	D-alanine bonded to the C-terminus
DEA	dissociative electron attachment
DN	D-alanine bonded to the N-terminus
ECD	electron circular dichroism
FTIR	Fourier transform infrared
HECO	high-energy cut-off in the LEPS spectrum
HREEL	high-resolution electron energy loss
IC	injection curve
IMS	intermolecular stabilization
LB	Langmuir−Blodgett
LC	L-alanine bonded to the C-terminus
LECO	low-energy cut-off in the LEPS spectrum
LEE	low-energy electron
LEET	low-energy electron transmission
LEPET	low-energy photoelectron transmission
LUMO	lowest unoccupied molecular orbital
MFP	mean free path
ML	monolayer
OOTF	organized organic thin film
QSE	quantum size effect
RS	resonance stabilization
SAM	self-assembled monolayer
ds	double-stranded
ss	single-stranded
TPPE	two-photon photoemission
UHV	ultrahigh vacuum
VL	vacuum level (i.e., zero energy reference)

14. Acknowledgment

We would like to thank Dr. Andrew Bass and Ms. Francine Lussier for their assistance in the preparation of this manuscript. This work was funded by the Canadian Institutes of Health Research. R.N. acknowledges the support of the Israel Science Foundation.

15. References

(1) Kuznetsov, A. M. *Charge Transfer in Physics, Chemistry and Biology*; Gordon and Breach: New York, 1995.
(2) (a) Carter, F. L. *Molecular Electronic Devices*; Marcel Dekker Inc.: New York, 1987. (b) Lehn, J. M. *Angew. Chem.* **1988**, *100*, 89. (c) *Molecular and Biomolecular electronics*; Birge, R. R., Ed.; American Chemical Society: Washington, DC, 1994. (d) Aviram, A.; Ratner, M. A. *Chem. Phys. Lett.* **1974**, *29*, 277. (e) *Molecular Electronics*; Jortner, J., Ratner, M., Eds.; Blackwell Science Ltd: Oxford, U.K., 1997.
(3) Harris, J. E., Ed. *Electron Microscopy in Biology: A Practical Approach*; IRL Press at Oxford University Press: Oxford, New York, Tokyo, 1991.
(4) Marsolais, R. M.; Cartier, E. A.; Pfluger, P. In *Excess Electrons in Dielectric Media*; Jay-Gerin, J.-P., Ferradini, C. Eds.; CRC Press: Boca Raton, FL, 1991; p 43.
(5) Naaman, R.; Vager, Z. *Acc. Chem. Res.* **2003**, *36*, 291.
(6) Bader, G.; Perluzzo, G.; Caron, L. G.; Sanche, L. *Phys. Rev. B* **1984**, *30*, 78.
(7) Holroyd, R. A.; Schmidt, W. F. *Annu. Rev. Phys. Chem.* **1989**, *40*, 439.
(8) Marcus, R. A. *J. Chem. Phys.* **1956**, *24*, 966. Marcus, R. A. *Oxidases and Related Redox Systems*; Pergamon Press: New York, 1982.
(9) Todd, M. D.; Nitzan, A.; Ratner, M. A.; Hupp, J. T. *J. Photochem. Photobiol.* **1994**, *82*, 87.
(10) Haran, A.; Kadyshevitch, A.; Cohen, H.; Naaman, R.; Evans, D.; Seidman, T.; Nitzan, A. *Chem. Phys. Lett.* **1997**, *268*, 475.
(11) Galperin, M.; Nitzan, A.; Benjamin, I. *J. Phys. Chem. A* **2002**, *106*, 10790.
(12) Nitzan, A. *Annu. Rev. Phys. Chem.* **2001**, *52*, 681.
(13) Hilsch, R. *Z. Phys.* **1932**, *77*, 427.
(14) Wright, D. A. *Br. J. Appl. Phys.* **1954**, *5*, 108.
(15) Bruning, H. In *Physics and Applications of Secondary Electron Emission*; Pergamon: London, 1954; p 93.
(16) Jacobs, H.; Greenberg, I. N.; Goble, L.; Ramsa, A. *Phys. Rev.* **1957**, *106*, 921.
(17) Fredrikov, S. A.; Goryacheva, G. N. *Izv. Akad. Nauk SSSR* **1958**, *22*, 486. *Bull. Acad. Sci. U.S.S.R.* **1958**, *22*, 491.
(18) Fredericks, W. J.; Cook, C. J. *Phys. Rev.* **1961**, *121*, 1693.
(19) Hiraoka, K.; Hamill, W. H. *J. Chem. Phys.* **1972**, *56*, 3185; **1972**, *57*, 4058.
(20) Huang, T.; Hamill, W. H. *J. Chem. Phys.* **1974**, *61*, 3144.
(21) Hiraoka, K.; Hamill, W. H. *J. Chem. Phys.* **1973**, *58*, 3686.
(22) Huang, T.; Hamill, W. H. *J. Phys. Chem. Solids* **1975**, *36*, 661.
(23) Hiraoka, K.; Hamill, W. H. *J. Chem. Phys.* **1972**, *57*, 3870.
(24) Hiraoka, K.; Hamill, W. H. *J. Chem. Phys.* **1973**, *59*, 5749.
(25) Hiraoka, K.; Nara, M. *Bull. Chem. Soc. Jpn.* **1981**, *54*, 1589; **1981**, *54*, 3317.
(26) Sanche, L. *J. Chem. Phys.* **1979**, *71*, 4860.
(27) Sanche, L. *J. Phys. C.* **1980**, *13*, L677; *Chem. Phys. Lett.* **1979**, *65*, 61.
(28) Perluzzo, G.; Bader, G.; Caron, L. G.; Sanche, L. *Phys. Rev. Lett.* **1985**, *55*, 545.
(29) Zhu, Q.-G.; Yang, Y.; Williams, E. D.; Park, R. L. *Phys. Rev. Lett.* **1987**, *59*, 835.

(30) Jonker, B. T.; Park, R. L. *Surf. Sci.* **1984**, *146*, 93; **1984**, *146*, 511.
(31) Hiraoka, K.; Nara, M. *Bull. Chem. Soc. Jpn.* **1984**, *57*, 2243.
(32) Jaklevis, R. C.; David, L. C. *Phys. Rev. B* **1982**, *26*, 5391.
(33) Plenkiewicz, B.; Plenkiewicz, P.; Perluzzo, G.; Jay-Gerin, J.-P. *Phys. Rev. B* **1985**, *32*, 1253.
(34) Komolov, A.; Moller, P. J. *Appl. Surf. Sci.* **2005**, *244*, 573.
(35) Marsolais, R. M.; Michaud, M.; Sanche, L. *Phys. Rev. A* **1987**, *35*, 607.
(36) Ueno, N.; Sugita, K.; Seki, K.; Inokuchi, H. *Phys. Rev. B* **1986**, *34*, 6386.
(37) Ueno, N.; Azuma, Y.; Yokota, T.; Aoki, M.; Okudaira, K. K.; Harada, Y. *Jpn. J. Appl. Phys. Part 1* **1997**, *36*, 5731 and references therein.
(38) Momose, M.; Kamiya, K.; Sugita, K.; Ueno, N. *Jpn. J. Appl. Phys. Part 1* **1994**, *33*, 4754.
(39) Perluzzo, G.; Sanche, L.; Gaubert, C.; Baudoing, R. *Phys. Rev. B* **1984**, *30*, 4292.
(40) Ito, K.; Kera, S.; Okudaira, K. K.; Ueno, N. *J. Appl. Phys.* **2002**, *92*, 5203.
(41) Sanche, L.; Bader, G.; Caron, L. G. *J. Chem. Phys.* **1982**, *76*, 4016.
(42) Jonker, B. T.; Bartelt, N. C.; Park, R. L. *Surf. Sci.* **1983**, *127*, 183.
(43) Caron, L. G.; Perluzzo, G.; Bader, G.; Sanche, L. *Phys. Rev. B* **1985**, *33*, 3027.
(44) Keszei, E.; Jay-Gerin, J.-P.; Perluzzo, G.; Sanche, L. *J. Chem. Phys.* **1987**, *85*, 7936.
(45) Bader, G.; Perluzzo, G.; Caron, L. G.; Sanche, L. *Phys. Rev. B* **1982**, *26*, 6019.
(46) Hiraoka, K.; Nara, M. *J. Phys. Chem.* **1982**, *86*, 442.
(47) Hiraoka, K. *J. Phys. Chem.* **1981**, *85*, 4008.
(48) Marsolais, R. M.; Deschênes, M.; Sanche, L. *Rev. Sci. Instrum.* **1989**, *60*, 2724.
(49) Bass, A. D.; Parenteau, L.; Weik, F.; Sanche, L. *J. Chem. Phys.* **2000**, *113*, 8746.
(50) Komolov, A.; Moller, P. J. *Colloids Surf., A* **2004**, *239*, 49.
(51) Shayegan, M.; Cavallo, J. M.; Glover, R. E., III; Park, R. L. *Phys. Rev. Lett.* **1984**, *53*, 1578.
(52) Steinberger, I. T.; Bass, A. D.; Shechter, R.; Sanche, L. *Phys. Rev. B* **1993**, *48*, 8290.
(53) For application to high-resolution electron-energy-loss spectroscopy, see: Sanche, L.; Michaud, M. *Phys. Rev. B* **1984**, *30*, 6078. For application to electron-stimulated desorption, see: Sanche, L. *Phys. Rev. Lett.* **1984**, *53*, 1638.
(54) Berry, W. B. *J. Electrochem. Soc.* **1971**, *118*, 597.
(55) Chang, Y. C.; Berry, W. B. *J. Chem. Phys.* **1974**, *61*, 2727.
(56) Huang, J.-T. J.; Magee, J. L. *J. Chem. Phys.* **1974**, *61*, 2736.
(57) Pong, W.; Smith, J. A. *J. Appl. Phys.* **1973**, *44*, 174.
(58) Belkind, A. I.; Aleksandrov, S. B.; Aleksandrov, V. V. Presented at the Electrical Properties of Organic Solids Conference; Karpacz, Poland, 1974.
(59) Nielsen, P.; Sandman, D. J.; Epstein, A. J. *Solid State Commun.* **1975**, *17*, 1067.
(60) Lin, S. F.; Spicer, W. E.; Schechtman, B. H. *Phys. Rev. B* **1975**, *12*, 4184.
(61) Hino, S.; Sato, N.; Inokuchi, H. *Chem. Phys. Lett.* **1976**, *37*, 494.
(62) Hino, S.; Sato, N.; Inokuchi, H. *J. Chem. Phys.* **1977**, *67*, 4139.
(63) Pfluger, P.; Zeller, H. R.; Bernasconi, J. *Phys. Rev. Lett.* **1984**, *53*, 94.
(64) Seah, M. P.; Dench, W. A. *Surf. Interface Anal.* **1979**, *1*, 2.
(65) Kurtz, R. L.; Usuki, N.; Stockbauer, R.; Madeay, T. E. *J. Electron Spectrosc. Relat. Phenom.* **1986**, *40*, 35.
(66) Hupfer, B.; Schupp, H.; Andrade, J. D.; Ringsdorf, H. *J. Electron Spectrosc. Relat. Phenom.* **1981**, *23*, 103.
(67) Brundle, C. R.; Hopster, H.; Swalen, J. D. *J. Chem. Phys.* **1979**, *70*, 5190.
(68) Cadman, P.; Gossedge, G.; Scott, J. D. *J. Electron Spectrosc. Relat. Phenom.* **1978**, *13*, 1.
(69) Clark, D. T.; Thomas, H. R. *J. Polym. Sci., Polym. Chem. Ed.* **1977**, *15*, 2843.
(70) Cartier, E.; Pfluger, P. *Appl. Phys. A* **1987**, *44*, 43.
(71) Leyvy, L., Gardona, M., Eds. *Photoemission in Solids*; Springer: Berlin, 1979; p 264.
(72) Grechov, V. V.; Belkind, A. I. *Izv. Akad. Nauk. Latv. SSR Ser. Fiz. Tekh. Nauk* **1975**, *4*, 25.
(73) Ritsko, I. J.; Nielsen, P.; Miller, I. S. *J. Chem. Phys.* **1977**, *67*, 687.
(74) Grechov, V. V. *Chem. Phys. Lett.* **1983**, *96*, 237.
(75) Jo, S. K.; White, J. M. *J. Chem. Phys.* **1991**, *94*, 5761.
(76) Ge, N.-H.; Wong, C. M.; Harris, C. B. *Acc. Chem. Res.* **2000**, *33*, 111. Harris, C. B.; Ge, N.-H.; Lingle, R. L., Jr.; McNeil, J. D.; Wong, C. M. *Annu. Rev. Phys. Chem.* **1997**, *48*, 711.
(77) Wong, C. M.; McNeill, J. D.; Gaffney, K. J.; Ge, N.-H.; Miller, A. D.; Liu, S. H.; Harris, C. B. *J. Phys. Chem. B* **1999**, *103*, 282.
(78) Wang, H.; Dutton, G.; Zhu, X.-Y. *J. Phys. Chem. B* **2000**, *104*, 10332. Zhu, X.-Y. *Annu. Rev. Phys. Chem.* **2002**, *53*, 221.
(79) Vondrak, T.; Cramer, C. J.; Zhu, X.-Y. *J. Phys. Chem. B* **1999**, *103*, 8915.
(80) Lingle, R. L., Jr.; Padowitz, D. F.; Jordan, R. E.; McNeill, J. D.; Harris, C. B. *Phys. Rev. Lett.* **1994**, *72*, 2243.
(81) Zhong, Q.; Gahl, C.; Wolf, M. *Surf. Sci.* **2002**, *496*, 21.
(82) Leclerc, G.; Goulet, T.; Cloutier, P.; Jay-Gerin, J.-P.; Sanche, L. *J. Phys. Chem.* **1987**, *91*, 4999.
(83) Stamatovic, A.; Schulz, G. J. *Rev. Sci. Instrum.* **1970**, *41*, 423. Roy, D. *Rev. Sci. Instrum.* **1972**, *43*, 535.
(84) Burrow, P. D.; Sanche, L. *Phys. Rev. Lett.* **1972**, *28*, 333.
(85) Kadyshevitch, A.; Naaman, R. *Phys. Rev. Lett.* **1995**, *74*, 3443.
(86) Kadyshevitch, A.; Naaman, R. *Thin Solid Films* **1996**, *288*, 139.
(87) Kadyshevitch, A.; Naaman, R. *Surf. Interface Anal.* **1997**, *25*, 71.
(88) Plenkiewicz, P.; Plenkiewicz, B.; Jay-Gerin, J.-P. *Phys. Rev. B* **1986**, *33*, 5744.
(89) (a) Jay-Gerin, J.-P.; Plenkiewicz, B.; Plenkiewicz, P.; Perluzzo, G.; Sanche, L. *Solid State Commun.* **1985**, *55*, 1115. (b) Keszei, E.; Jay-Gerin, J.-P.; Perluzzo, G.; Sanche, L. *J. Chem. Phys.* **1986**, *85*, 7396.
(90) Goulet, T.; Jay-Gerin, J.-P. *Radiat. Phys. Chem.* **1986**, *27*, 229. Goulet, T.; Pou, V.; Jay-Gerin, J.-P. *J. Electron Spectrosc. Relat. Phenom.* **1986**, *41*, 157. Goulet, T.; Jay-Gerin, J.-P.; Patau, J.-P. *J. Electron Spectrosc. Relat. Phenom.* **1987**, *43*, 17.
(91) Goulet, T.; Keszei, E.; Jay-Gerin, J.-P. *Phys. Rev. A* **1988**, 37, 2176. Keszei, E.; Goulet, T.; Jay-Gerin, J.-P. *Phys. Rev. A* **1988**, *37*, 2183.
(92) Plenkiewicz, P.; Jay-Gerin, J.-P.; Plenkiewicz, B.; Perluzzo, G. *Solid State Commun.* **1986**, *57*, 203.
(93) Plenkiewicz, P.; Plenkiewicz, B.; Jay-Gerin, J.-P. *Solid State Commun.* **1988**, *65*, 1227.
(94) Harrigan, M. E.; Lee, H. J. *J. Chem. Phys.* **1974**, *60*, 4909.
(95) Cheng, I. Y.; Funabashi, K. *J. Chem. Phys.* **1973**, *59*, 2977.
(96) Perluzzo, G.; Bader, G.; Caron, L. G.; Sanche, L. *Phys. Rev. B* **1982**, *26*, 3976.
(97) Michaud, M.; Sanche, L.; Gaubert, C.; Baudoing, R. *Surf. Sci.* **1988**, *205*, 447.
(98) Komolov, S. A.; Lazneva, E. F.; Komolov, A. S. *Tech. Phys. Lett.* **2003**, *29*, 974.
(99) Komolov, A. S.; Moller, P. J. *Synth. Met.* **2003**, *138*, 119.
(100) Sanche, L.; Perluzzo, G.; Bader, G.; Caron, L. G. *J. Chem. Phys.* **1982**, *77*, 3285.
(101) Resca, L.; Rodriguez, S. *Phys. Rev. B* **1978**, *17*, 3334.
(102) Schwentner, N. *Phys. Rev. B* **1976**, *14*, 5490. Klein, M. L.; Koehler, T. R. In *Rare Gas Solids*; Klein, M. L., Venables, J. A., Eds.; Academic Press: New York, 1976; p 301.
(103) Rath, J.; Freeman, A. J. *Phys. Rev. B* **1975**, *11*, 2109.
(104) Fujihira, M.; Inokuchi, H. *Chem. Phys. Lett.* **1972**, *17*, 554.
(105) Ueno, N.; Sugita, K. *Solid State Commun.* **1980**, *34*, 355.
(106) Michaud, M.; Cloutier, P.; Sanche, L. *Phys. Rev. B* **1991**, *44*, 10485.
(107) Michaud, M.; Cloutier, P.; Sanche, L. *Phys. Rev. B* **1994**, *49*, 8360.
(108) Bacalis, N. C.; Papaconstantopoulos, D. A.; Pickett, W. E. *Phys. Rev. B* **1988**, *38*, 6218.
(109) Peterson, O. G.; Batchelder, D. N.; Simmons, R. O. *Phys. Rev.* **1966**, *150*, 703.
(110) Ray, A. K.; Trickey, S. B. *Phys. Rev. B* **1981**, *24*, 1751.
(111) Ray, A. K.; Trickey, S. B. *Phys. Rev. B* **1983**, *28*, 7352.
(112) Michaud, M.; Sanche, L.; Goulet, T.; Jay-Gerin, J.-P. *Phys. Rev. Lett.* **1991**, *66*, 1930.
(113) Michaud, M.; Sanche, L. *Phys. Rev. A* **1987**, *36*, 4684.
(114) Michaud, M.; Sanche, L. *Phys. Rev. B* **1984**, *30*, 6067.
(115) Kittel, C. *Quantum Theory of Solids*; Wiley: New York, 1963; p 137.
(116) Sanche, L. In *Excess Electrons in Dielectric Media*, Ferradini, C., Jay-Gerin, J.-P., Eds.; CRC: Boca Raton, FL, 1991.
(117) Bass, A. D.; Sanche, L. *Radiat. Environ. Biophys.* **1998**, *37*, 243.
(118) Hager, S. L.; Willard, J. E. *J. Chem. Phys.* **1975**, *63*, 942.
(119) Takeda, K.; Oguni, M.; Suga, H. *J. Phys. Chem. Solids* **1991**, *52*, 991.
(120) Nagesha, K.; Sanche, L. *Phys. Rev. Lett.* **1998**, *81*, 5892.
(121) Sanche, L. *Scanning Microsc.* **1995**, *9*, 619.
(122) Sanche, L.; Michaud, M. *Phys. Rev. B* **1983**, *27*, 3856.
(123) Demuth, J. E.; Schmeisser, D.; Avouris, Ph. *Phys. Rev. Lett.* **1981**, *47*, 116.
(124) Sanche, L.; Michaud, M. *Chem. Phys. Lett.* **1981**, *84*, 49.
(125) Schulz, G. J. *Rev. Mod. Phys.* **1973**, *45*, 423.
(126) Ehrhardt, H.; Willmann, K. *Z. Phys.* **1967**, *204*, 462.
(127) Tronc, M.; Azria, R.; Le Coat, Y. *J. Phys. B* **1980**, *13*, 2327.
(128) Fano, U.; Stevens, J. A. *Phys. Rev. B* **1986**, *34*, 438.
(129) See, for example, Messiah, A. *Mécanique Quantique*; Dunod: Paris, 1964.
(130) Ashby, C. I. H. *Appl. Phys. Lett.* **1983**, *43*, 609.
(131) Hall, R. I.; Mazeau, J.; Reinhardt, J.; Schermann, C. *J. Phys. B* **1970**, *3*, 991.
(132) Goulet, T.; Jay-Gerin, J.-P. *Solid State Commun.* **1985**, *55*, 619.

(133) Leclerc, G.; Goulet, T.; Cloutier, P.; Jay-Gerin, J.-P.; Sanche, L. *Can. J. Phys.* **1987**, *65*, 1133.
(134) Goulet, T.; Keszei, E.; Jay-Gerin, J.-P. *Phys. Rev. A* **1990**, *41*, 6006.
(135) Keszei, E.; Marsolais, R.; Deschênes, M.; Goulet, T.; Sanche, L.; Jay-Gerin, J.-P. *J. Electron Spectrosc. Relat. Phenom.* **1989**, *49*, 175.
(136) Keszei, E.; Cobut, V.; Jay-Gerin, J.-P. *J. Electron Spectrosc. Relat. Phenom.* **1992**, *58*, 33.
(137) Dwyer, V. M. *Phys. Rev. A* **1993**, *47*, 3044.
(138) Sambe, H.; Ramaker, D. E.; Deschênes, M.; Bass, A. D.; Sanche, L. *Phys. Rev. Lett.* **1990**, *64*, 523.
(139) Sanche, L.; Deschênes, M. *Phys. Rev. Lett.* **1988**, *61*, 2096.
(140) Bass, A. D.; Sanche, L. *J. Chem. Phys.* **1991**, 95, 2910.
(141) Bass, A. D.; Gamache, J.; Parenteau, L.; Sanche, L. *J. Phys. Chem.* **1995**, *99*, 6123.
(142) Huels, M. A.; Bass, A. D.; Ayotte, P.; Sanche, L. *Chem. Phys. Lett.* **1995**, *245*, 387.
(143) Sanche, L.; Bass, A. D.; Ayotte, P.; Fabrikant, I. I. *Phys. Rev. Lett.* **1995**, *75*, 3568.
(144) Bass, A. D.; Gamache, J.; Ayotte, P.; Sanche, L. *J. Chem. Phys.* **1996**, *104*, 4258.
(145) Ayotte, P.; Gamache, J.; Bass, A. D.; Fabrikant, I. I.; Sanche, L. *J. Chem. Phys.* **1997**, *106*, 749.
(146) Bass, A. D.; Lezius, M.; Ayotte, P.; Parenteau, L.; Cloutier, P.; Sanche, L. *J. Phys. B: At., Mol. Opt. Phys.* **1997**, *30*, 3527.
(147) Nagesha, K.; Sanche, L. *Phys. Rev. Lett.* **1997**, *78*, 4725.
(148) Fabrikant, I. I.; Nagesha, K.; Wilde, R.; Sanche, L. *Phys. Rev. B* **1997**, *56*, R5725.
(149) Weik, F.; Illenberger, E.; Nagesha, K.; Sanche, L. *J. Phys. Chem. B* **1997**, *102*, 824.
(150) Massey, H. S. W. *Negative ions*, 3rd ed.; Cambridge University: Cambridge, U.K., 1976.
(151) Simpson, W. C.; Orlando, T. M.; Parenteau, L.; Nagesha, K.; Sanche, L. *J. Chem. Phys.* **1998**, *108*, 5027.
(152) Rowntree, P.; Sanche, L.; Parenteau, L.; Meinke, M.; Weik, F.; Illenberger, E. *J. Chem. Phys.* **1994**, *101*, 4248.
(153) Tegeder, P.; Kendall, P. A.; Penno, M.; Mason, N. J.; Illenberger, E. *Phys. Chem. Chem. Phys.* **2001**, *3*, 2625.
(154) Lu, Q. B.; Sanche, L. *J. Chem. Phys.* **2001**, *115*, 5711.
(155) Meinke, M.; Illenberger, E. *J. Phys. Chem.* **1994**, *98*, 6601.
(156) Meinke, M.; Parenteau, L.; Rowntree, P.; Sanche, L.; Illenberger, E. *Chem. Phys. Lett.* **1993**, *205*, 213.
(157) Oster, T.; Ingolfsson, O.; Meinke, M.; Jaffke, J.; Illenberger, E. *J. Chem. Phys.* **1993**, *99*, 5141.
(158) Weik, F.; Illenberger, E. *J. Chem. Phys.* **1995**, *103*, 1406. Ingolfsson, O.; Weik, F.; Illenberger, E. *Int. Rev. Phys. Chem.* **1996**, *15*, 133.
(159) Tegeder, P.; Bruning, F.; Illenberger, E. *Chem. Phys. Lett.* **1999**, *310*, 79.
(160) Le Coat, Y.; Hedhili, N. M.; Azria, R.; Tronc, M.; Weik, F.; Illenberger, E. *Int. J. Mass Spectrom. Ion Processes* **1997**, *164*, 231.
(161) Bruning, F.; Tegeder, P.; Langer, J.; Illenberger, E. *Int. J. Mass Spectrom.* **2000**, *196*, 507.
(162) Tegeder, P.; Smirnov, B. M.; Illenberger, E. *Int. J. Mass Spectrom.* **2001**, *205*, 331.
(163) Langer, J.; Matt, S.; Meinke, M.; Tegeder, P.; Stamatovic, A.; Illenberger, E. *J. Chem. Phys.* **2000**, *113*, 11063.
(164) Le Coat, Y.; Azria, R.; Tronc, M.; O. Ingolfsson; Illenberger, E. *Chem. Phys. Lett.* **1998**, *296*, 208.
(165) Tegeder, P.; Illenberger, E. *Chem. Phys. Lett.* **2001**, *341*, 401.
(166) Weik, F.; Illenberger, E.; Nagesha, K.; Sanche, L. *J. Phys. Chem. B* **1998**, *102*, 824.
(167) Nagesha, K.; Sanche, L. *J. Appl. Phys.* **2000**, *88*, 5211.
(168) Nagesha, K.; Fabrikant, I. I.; Sanche, L. *J. Chem. Phys.* **2001**, *114*, 4934.
(169) Weik, F.; Sanche, L.; Ingolfsson, O.; Illenberger, E. *J. Chem. Phys* **2000**, *112*, 9046.
(170) Lu, Q.-B.; Madey, T. E. *J. Chem. Phys.* **1999**, *111*, 2861.
(171) Lu, Q.-B.; Madey, T. E. *Phys. Rev. Lett.* **1999**, 82, 4122; *Surf. Sci.* **2000**, *451*, 238.
(172) Lu, Q.-B.; Sanche, L. *Phys. Rev. B* **2001**, *63*, 153403.
(173) Christophorou, L. G.; Stockdale, J. A. *J. Chem. Phys.* **1968**, *48*, 1956. Illenberger, E.; Scheunemann, H.-U.; Baugartel, H. *Chem. Phys.* **1979**, *37*, 21.
(174) Lu, Q.-B.; Sanche, L. *Phys. Rev. Lett.* **2001**, *87*, 078501.
(175) Kadyshevitch, A.; Ananthavel, S. P.; Naaman, R. *J. Chem. Phys.* **1997**, *107*, 1288.
(176) Segev, L.; Salomon, A.; Natan, A.; Cahen. D.; Kronik, L.; Amy, F.; Chan, C. K.; Kahn, A. *Phys. Rev. B*, in press.
(177) Sun, C.-K.; Valle, F.; Acioli, L. H.; Ippen, E. P.; Fujimoto, J. G. *Phys. Rev. B* **1994**, *50*, 15337.
(178) Arifov, U. A.; Kazanskii, V. V.; Lugovskoi, V. B.; Makarenko, V. A. *Dokl. Akad. Nauk. SSSR* **1969**, *9*, 18.
(179) Charalambidis, D.; Hontzopoulos, E.; Fotakis, C.; Farkas, Gy.; Toth, Cs. *J. Appl. Phys.* **1989**, *65*, 2843.
(180) Damascelli, A.; Gabetta, G.; Lumachi, A.; Fini, L.; Parmigiani, F. *Phys. Rev. B* **1996**, *54*, 6031.
(181) Lugovskoy, A. V.; Usmanov, T.; Zinoviev, A. V. *J. Opt. Soc. Am. B* **1998**, *15*, 53.
(182) Chen, Y. F. *Phys. Rev. B* **1997**, *55*, 5478.
(183) Samartzis, P. C.; Sakellariou, I.; Gougousi, T.; Kitsopoulos, T. N. *J. Chem. Phys.* **1997**, *107*, 43.
(184) Dimitrov, S.; Trakhtenberg, S.; Naaman, R.; Smith, D. J.; Samartzis, P. C.; Kitsopoulos, T. N. *Chem. Phys. Lett.* **2000**, *322*, 587.
(185) Osiander, R.; Korpium, P.; Duschl, C.; Knoll, W. *Thin Solid Films* **1988**, *160*, 501.
(186) Gemmel, D. *Rev. Mod. Phys.* **1974**, *46*, 129.
(187) ICRU Report Vol. 31, International Commission on Radiation Units and Measurements, Washington, DC, 1979.
(188) Pimblott, S. M.; LaVerne, J. A. *Radiation Damage in DNA: Structure/Function Relationships at Early Time*; Fuciarelli, A. F., Zimbrick, J. D., Eds.; Battelle: Columbus, OH, 1995; Chapter 1.
(189) Boudaiffa, B.; Cloutier, P.; Hunting, D.; Huels, M. A.; Sanche, L. *Science* **2000**, *287*, 1658.
(190) Barrios, R.; Skurski, P.; Simons, J. *J. Phys. Chem. B* **2002**, *106*, 7991.
(191) Abdoul-Carime, H.; Sanche, L. *Int. J. Radiat. Biol.* **2002**, *78*, 89.
(192) Ray, S. G.; Daube, S. S.; Naaman, R. *Proc. Natl. Acad. Sci. U.S.A.* **2005**, *102*, 15.
(193) Williamson, J. R. *Annu. Rev. Biophys. Biomol. Struct.* **1994**, *23*, 703.
(194) Wong, K. K.; Chang, S.; Weiler, S. R.; Ganesan, S.; Chaudhuri, J.; Zhu, C. M.; Artandi, S. E.; Rudolph, K. L.; Gottlieb, G. J.; Chin, L.; Alt, F. W.; DePinho, R. A. *Nat. Genet.* **2000**, *26*, 85.
(195) Steenken, S.; Jovanovic, S. V. *J. Am. Chem. Soc.* **1997**, *119*, 617.
(196) Milligan, J. R.; Aguilera, J. A.; Ward, J. F. *Int. J. Radiat. Biol.* **2001**, *77*, 1195.
(197) Giese, B.; Amaudrut, J.; Kohler, A. K.; Spormann, M.; Wessely, S. *Nature* **2001**, *412*, 318.
(198) Schuster, G. B. *Acc. Chem. Res.* **2000**, *33*, 253, 631.
(199) Jortner, J.; Bixon, M.; Langenbacher, T.; Michel-Beyerle, M. E. *Proc. Natl. Acad. Sci. U.S.A.* **1998**, *95*, 12759.
(200) Berlin, Y. A.; Burin, A. L.; Ratner, M. A. *J. Am. Chem. Soc.* **2001**, *123*, 260.
(201) Heller, A. *Faraday Discuss.* **2000**, 1.
(202) Friedman, K. A.; Heller, A. *J. Phys. Chem. B* **2001**, *105*, 11859.
(203) Aqua, T.; Naaman, R.; Daube, S. S. *Langmuir* **2003**, *19*, 10573.
(204) Petrovykh, D. Y.; Kimura-Suda, H.; Whitman, L. J.; Tarlov, M. J. *J. Am. Chem. Soc.* **2003**, *125*, 5219.
(205) Boudaiffa, B.; Cloutier, P.; Hunting, D.; Huels, M. A.; Sanche, L. *Radiat. Res.* **2002**, *157*, 227.
(206) Miller, A. D.; Bezel, I.; Gaffney, K. J.; Garrett-Roe, S.; Liu, S. H.; Szymanski, P.; Harris, C. B. *Science* **2002**, *297*, 1163.
(207) Hofer, U.; Shumay, I. L.; Reuss, C.; Thomann, U.; Wallauer, W.; Fauster, T. *Science* **1997**, *277*, 1480.
(208) Hush, N. S.; Cheung, A. S. *Chem. Phys. Lett.* **1975**, *34*, 11.
(209) Nir, E.; Grace, L.; Brauer, B.; de Vries, M. S. *J. Am. Chem. Soc.* **1999**, *121*, 4896.
(210) Wiley, J. R.; Robinson, J. M.; Ehdaie, S.; Chen, E. C. M.; Chen, E. S. D.; Wentworth, W. E. *Biochem. Biophys. Res. Commun.* **1991**, *180*, 841.
(211) Chen, E. S.; Chen, E. C. M. *Biochem. Biophys. Res. Commun.* **2001**, *289*, 421.
(212) Zhang, Q.; Chen, E. C. M. *Biochem. Biophys. Res. Commun.* **1995**, *217*, 755.
(213) Periquet, V.; Moreau, A.; Carles, S.; Schermann, J. P.; Desfrancois, C. *J. Electron Spectrosc. Relat. Phenom.* **2000**, *106*, 141.
(214) Aflatooni, K.; Gallup, G. A.; Burrow, P. D. *J. Phys. Chem. A* **1998**, *102*, 6205.
(215) Voityuk, A. A.; Michel-Beyerle, M.-E.; Rosch, N. *Chem. Phys. Lett.* **2001**, *342*, 231.
(216) Srivastava, S. K.; Mishra, P. C. *J. Mol. Struct.* **1980**, *65*, 199.
(217) Sabio, M.; Topiol, S.; Lumma, W. C. *J. Phys. Chem.* **1990**, *94*, 1366.
(218) Dolgounitcheva, O.; Zakrzewski, V. G.; Ortiz, J. V. *J. Phys. Chem. A* **2001**, *105*, 8782.
(219) Ray, S. G.; Cohen, H.; Naaman, R.; Rabin, Y. *J. Am. Chem. Soc.* **2005**, *127*, 17138.
(220) Dutton, G.; Zhu, X. Y. *J. Phys. Chem. B* **2001**, *105*, 10912.
(221) Newton, G. L.; Aguilera, J. A.; Ward, J. F.; Fahey, R. C. *Radiat. Res.* **1996**, *145*, 776.
(222) Spotheim-Maurizot, M.; Ruiz, S.; Sabattier, R.; Charlier, M. *Int. J. Radiat. Biol.* **1995**, *68*, 571.
(223) Minsky, A.; Shimoni, E.; Frenkiel-Krispin, D. *Nat. Rev. Mol. Cell Biol.* **2002**, *3*, 50.
(224) Vester, F.; Ulbricht, T. L. V. *Naturwissenschaften* **1959**, *46*, 68.
(225) Mayer, S.; Kessler, J. *Phys. Rev. Lett.* **1995**, *74*, 4803.
(226) Ray, K.; Ananthavel, S. P.; Waldeck, D. H.; Naaman, R. *Science* **1999**, *283*, 814.

(227) Kirschner, J. *Polarized Electrons at Surfaces*; Springer-Verlag, 1985. Meier, F.; Pescia, D. *Phys. Rev. Lett.* **1981**, *47*, 374. Meier, F.; Bona, G. L.; Hufner, S. *Phys. Rev. Lett.* **1984**, *52*, 1152. Borstel, G.; Wohlecke, M. *Phys. Rev. B* **1982**, *26*, 1148.
(228) Carmeli, I.; Skakalova, V.; Naaman, R.; Vager, Z. *Angew. Chem., Int. Ed.* **2002**, *41*, 761.
(229) Carmeli, I.; Skakalova, V.; Naaman, R.; Vager, Z. In *Biophysical Chemistry, Membranes and Protein*; Templer, R. H., Leatherbarrow, R., Eds.; Royal Society for Chemistry: Cambridge, U.K., 2002.
(230) Vager, Z.; Naaman, R. *Chem. Phys.* **2002**, *281*, 305.
(231) Carmeli, I.; Gefen, Z.; Vager, Z.; Naaman, R. *Phys. Rev. B* **2003**, *68*, 115418.
(232) Helenius, V.; Korppi-Tommola, J.; Kotila, S.; Nieminen, J.; Lohikoski, R.; Timonen, J. *Chem. Phys. Lett.* **1997**, *280*, 325. Careri, G.; Buontempo, U.; Carta, F.; Gratton, E.; Scott, A. C. *Phys. Rev. Lett.* **1983**, *51*, 304.
(233) Naaman, R.; Vager, Z. *Phys. Chem. Chem. Phys.* **2006**, *8*, 2217.
(234) Ray, S. G.; Daube, S. S.; Leitus, G.; Vager, Z.; Naaman, R. *Phys. Rev. Lett.* **2006**, *96*, 036101.
(235) Crespo, P.; Litran, R.; Rojas, T. C.; Multigner, M.; de la Fuente, J. M.; Sánchez-López, J. C.; García, M. A.; Hernando, A.; Penadés, S.; Fernández, A. *Phys. Rev. Lett.* **2004**, *93*, 087204.
(236) Yamamoto, Y.; Miura, T.; Suzuki, M.; Kawamura, N.; Miyagawa, H.; Nakamura, T.; Kobayashi, K.; Teranishi, T.; Hori, H. *Phys. Rev. Lett.* **2004**, *93*, 116801.
(237) Hori, H.; Teranishi, T.; Nakae, Y.; Seino, Y.; Miyake, M.; Yamada, S. *Phys. Lett. A* **1999**, *263*, 406. Hori, H.; Yamamoto, Y.; Iwamoto, T.; Miura, T.; Teranishi, T.; Miyake, M. *Phys. Rev. B* **2004**, *69*, 174411.
(238) Esquinazi, P.; Spemann, D.; Höhne, R.; Setzer, A.; Han, K.-H.; Butz, T. *Phys. Rev. Lett.* **2003**, *91*, 227201.
(239) Cahen, D.; Naaman, R.; Vager, Z. *Adv. Funct. Mater.* **2005**, *15*, 1571.
(240) Drouhin, H. J.; van der Sluijs, A. J.; Lassailly, Y.; Lampel, G. *J. Appl. Phys.* **1996**, *79*, 4734.
(241) Carmeli, I.; Leitus, G.; Naaman, R.; Reich, S.; Vager, Z. *J. Chem. Phys.* **2003**, *118*, 10372.
(242) Sanche, L. *IEEE Trans. Electr. Insul.* **1997**, *4*, 507.
(243) von Sonntag, C. *Free-Radical-Induced DNA Damage and its Repair*; Springer: Berlin, 2006.
(244) Davis, J. J.; Morgan, D. A.; Wrathmell, C. L.; Axford, D. N.; Zhao, J.; Wang, N. *J. Mater. Chem.* **2005**, *15*, 2160.
(245) Carmeli, I.; Leitus, G.; Naaman, R.; Reich, S.; Vager, Z. *Isr. J. Chem.* **2003**, *43*, 399.

CR040200J